Summer 2016

Quantitative computed tomography based measures of vascular dysfunction for identifying COPD phenotypes and subphenotypes

Timothy M. Dougherty
University of Iowa

QUANTITATIVE COMPUTED TOMOGRAPHY BASED MEASURES OF VASCULAR DYSFUNCTION FOR IDENTIFYING COPD PHENOTYPES AND SUBPHENOTYPES

by

Timothy M. Dougherty

A thesis submitted in partial fulfillment
of the requirements for the Master of Science
degree in Biomedical Engineering in the
Graduate College of
The University of Iowa

August 2016

Thesis Supervisor: Professor Eric A. Hoffman

Graduate College
The University of Iowa
Iowa City, Iowa

CERTIFICATE OF APPROVAL

_____

MASTER'S THESIS

_____

This is to certify that the Master's thesis of

Timothy M. Dougherty

has been approved by the Examining Committee for
the thesis requirement for the Master of Science degree
in Biomedical Engineering at the August 2016 graduation.

Thesis Committee: _____
Eric A. Hoffman, Thesis Supervisor

_____
Jessica C. Sieren

_____
Joseph M. Reinhardt

ACKNOWLEDGEMENTS

I have been very fortunate to have worked with many wonderful people in the Advanced Pulmonary Physiomic Imaging Laboratory the past two years. There are many people to thank and I don't want to miss anyone, so first I would like to give a general thank you to everyone I have worked with in the lab before addressing specific people/groups.

Thank you to my roommates, Zach and Andy, for your support, friendship and for knowing when I could use a break from work to clear my head with a quick game of League of Legends.

Thank you to Melissa, Shayna, Chelsea and Kelly for your assistance with animal studies and calendar trivia. I am more comfortable leading studies and horrible at trivia.

Thank you to previous graduate students Dr. Dr. Krishna Iyer for your training, knowledge and friendship. Data collection/analysis is much less monotonous with your stories. Thank you to Dr. Samantha Dilger for your wonderful insights, friendship and the wonderful little potato who made me believe I could do the thing.

Thank you to current graduate students Emily Hammond and Johanna Uthoff for your wit, friendship, and awesome movie soundtrack playlist. A special thank you to current graduate student Jacob Herrmann for assisting with MATLAB problems, helping with animal studies, sharing Imgur links and everything in between.

Lastly I would like to thank my thesis committee, especially my advisor, Dr. Eric Hoffman, for supporting me during my graduate studies, pushing me to think more critically and inspiring a deeper appreciation for science.

ABSTRACT

Chronic obstructive pulmonary disease (COPD) is a progressive, debilitating disease of the lung parenchyma and airways for which there is no cure. Most treatments are limited to the management of symptoms, which makes early detection more important if we are to begin to treat the disease etiology itself. Computed tomography is increasingly being used to diagnose, characterize and track COPD phenotypes such as small airways disease and emphysema.

In this thesis we follow-up on our earlier observations which suggested that vascular contraction (hypoxic pulmonary vasoconstriction) in patchy regions of inflammation of emphysema susceptible smokers promote emphysema advancement. In this study we take advantage of 1 year longitudinal data from quantitative computed tomography (QCT) to evaluate whether or not upstream pulmonary arterial dilation that accompanies down-stream vasoconstriction differentiates rapid emphysema progressors from non progressors. We demonstrate that arterial enlargement does predict rate of progression and is a marker of those subjects who at baseline already show signs of rapid progression amongst subjects with similar age and pack-year histories of smoking.

To further our ability to use dual energy computed tomography (DECT) with the context of longitudinal and multi-center studies we have established a low radiation dose DECT perfusion blood volume (PBV) imaging protocol with diluted contrast injection, taking advantage of advanced features of the Siemens SOMATOM Force DECT scanner.. In this study, we show that we can reduce the radiation dose by up to 34% without compromising our PBV heterogeneity measurement.

Finally, we use DECT PBV imaging to compare perfusion heterogeneity in a multi-center study where both GE (750HD) and Siemens (SOMATOM Force and Definition Flash) scanners are employed. In this analysis, we show that PBV heterogeneity is greater in regions of the lung showing signs of emphysema, but the most important factor appears to be the model DECT scanner used with the GE scanner exhibiting significantly greater image noise which translates to increased PBV heterogeneity estimates

PUBLIC ABSTRACT

Chronic obstructive pulmonary disease (COPD) is a debilitating lung disease almost exclusively related to tobacco smoke. COPD symptoms are typical of numerous other ailments making it difficult to diagnose and track. Technological advancements in CT imaging have allowed clinicians and researchers to expand simple structural information to functional information. These advancements have helped to increase the use of CT imaging in the study of smoking related lung disease.

In this thesis, we investigate observations from a previous study which suggested pulmonary artery constriction in inflamed lung regions promotes emphysema progression in smokers susceptible to emphysema. We use CT data from a 1 year longitudinal study to evaluate the pulmonary artery dimensions in rapid and non-progressing emphysema subjects. We show that the enlargement of arteries predicts emphysema progression and can be used to identify subjects showing signs of rapid emphysema progression.

We attempt to further our ability to use dual energy computed tomography (DECT) for longitudinal and multi-center studies by developing a DECT perfusion blood volume (PBV) imaging protocol with low radiation dose and diluted contrast. We demonstrate that we can reduce radiation dose by up to 34% with the advanced technology of Siemens SOMATOM Force scanner.

Finally, we use DECT PBV imaging to compare perfusion heterogeneity in a multi-center study with both GE and Siemens scanners. We show that perfusion heterogeneity is increased in lung regions showing signs of emphysema, but scanner

model/manufacturer appears to be the most important factor as data from the GE scanner had greater noise and thus increased perfusion heterogeneity.

TABLE OF CONTENTS

LIST OF TABLES

LIST OF FIGURES

CHAPTER 1: MOTIVATION AND RATIONALE

Chronic obstructive pulmonary disease (COPD) is a progressive, debilitating respiratory disease which is primarily caused by cigarette smoking in the United States. Most treatments for COPD involve managing symptoms with nebulizers and inhalers. Chronic bronchitis, peripheral small airways disease and emphysema are forms of COPD which may occur separately, however most patients present with some degree of both chronic bronchitis and emphysema [1, 2]. Emphysema is characterized as the enlargement of alveoli and destruction of small airways that is thought to be irreversible. CT imaging is increasingly being used to study smoking-related lung disease [1, 2]. Hoffman and colleagues [3, 4] have used functional CT imaging to demonstrate that normal smokers with early CT signs of emphysema susceptibility have twice the heterogeneity of pulmonary parenchymal perfusion compared to normal smokers without CT-based evidence of emphysema susceptibility [3] and the observed increased heterogeneity of perfusion is reversible with sildenafil [4]. Iyer et al, also demonstrated that the increased perfusion heterogeneity in emphysema susceptible smokers was associated with up-stream arterial dilation. As a follow-up to these studies we have taken advantage of the NIH sponsored SPIROMICS multi-center cohort [5] whereby smokers were studied via quantitative computed tomography at baseline and at a one year follow-on visit. Using this cohort we have sought to:

(1) Identify two subsets of SPIROMICS subjects based on rate of progression of emphysema (rapid progressors (RP) and non-progressors (NP)) and to evaluate central pulmonary arterial dimensions within the two groups. We

hypothesize that RP subjects will have enlarged central pulmonary arteries, indicative of downstream hypoxic vasoconstriction.

With the desire to facilitate the assessment of down-stream perfusion heterogeneity with the context of a longitudinal multi-center study we have:

(2) Developed a DE-PBV imaging protocol using a large animal model to quantitatively assess the effect of radiation dose reduction on PBV metrics. Determine the lowest radiation dose we can use to evaluate PBV heterogeneity without subjecting our data to significant noise in an effort to provide a framework for a low dose clinical DE imaging protocol.

Finally, to understand the generalizability of our imaging methodology, we have:

(3) Compared the DECT-based PBV heterogeneity measurements in a group of subjects studied with SPIROMICS on either a GE 750HD or a Siemens SOMATOM Force compared with our earlier studies on a Siemens Definition Flash scanner.

1.1 Lung Structure and Function

1.1.1 Airways and Alveoli

The primary function of the respiratory system is gas exchange. Outside air passes through the trachea and bronchi to lobar, segmental, sub-segmental and progressively smaller airways until reaching the terminal bronchioles, the smallest airways in the lungs that do not contain alveoli [6]. The purpose of these airways is to conduct air and is aptly named the conducting zone. Respiratory bronchioles, alveolar

ducts and sacs form the lung parenchyma in the respiratory zone, the site of gas exchange [6].

The parenchyma accounts for most of the lung's volume, meaning the lung is primarily composed of alveoli and capillaries. An alveolus consists of the air space, alveolar wall and pulmonary capillaries [6]. Gases are exchanged across a thin layer called the blood-gas barrier which is composed of alveolar endothelium, interstitium and capillary endothelium. Diffusion of gas occurs rapidly due to the large number of alveoli/capillaries and the thin blood-gas barrier [6].

1.1.2 Pulmonary Circulation

Pulmonary circulation starts from the right ventricle of the heart and ends at the left atrium. The pulmonary circuit is a low pressure system (5-20 mmHg) [6], unlike the systemic circuit (80-120 mmHg). Deoxygenated blood from the right ventricle is ejected into the main pulmonary artery and then diverted through the right and left pulmonary arteries which split into smaller arteries and arterioles, closely following the branching of the airways.

The pulmonary arteries consist of main pulmonary arteries down to the small muscular arteries and arterioles. Smooth muscle cells in these vessels control vascular tone and subsequently distribution of blood flow through changes in resistance of the vessels. Pulmonary capillaries form a dense network around the alveoli [7, 8]. The capillaries lead to the pulmonary venules and veins. These vessels carry oxygenated blood and to the left atrium.

1.1.3 Chronic Obstructive Pulmonary Disease

Chronic obstructive pulmonary disease (COPD) is a progressive, debilitating disease of the airways and lung parenchyma affecting millions of people worldwide. The World Health Organization (WHO) lists COPD as the 4th leading cause of death. COPD is primarily related to cigarette smoking in developed countries. Smokers make up 90% of COPD cases in the world [9].

Chronic bronchitis is a form of COPD occurring in the airways. Excessive mucus secretion is characteristic of chronic bronchitis and obstructs the lumen of the airway [10]. Emphysema is another form of COPD occurring in the lung parenchyma. Dilation of air spaces distal to the terminal bronchioles is characteristic of emphysema (Figure 1). Air spaces increase in size as alveolar walls and pulmonary capillaries are destroyed. Symptoms of COPD include cough, sputum production, chest tightness, shortness of breath and exacerbation, a sudden worsening of COPD symptoms which may last several days [10]. Most patients with COPD present characteristics of chronic bronchitis and emphysema, making it a heterogeneous disease [1, 2]. In addition, COPD has been linked with cardiovascular disease, diabetes and osteoporosis [10] and many symptoms of COPD are characteristic of other diseases and thus, COPD is often undiagnosed until it has progressed into moderate COPD.

COPD severity has been standardized by the Global initiative for chronic Obstructive Lung Disease (GOLD) [9]. GOLD classifies COPD into five stages from 0 (at risk for COPD) to 4 (very severe COPD) (Table 1). According to this classification, GOLD stages were determined by COPD symptoms (cough and sputum production) and spirometry results [9]. Spirometry measures include forced expiratory volume in 1 second

(FEV_1), forced vital capacity (FVC) and percent of predicted FEV_1 ($\%FEV_1$). Using this classification, FEV_1/FVC ratio determined COPD status (less than 70%) and $\%FEV_1$ determined the severity of COPD.

1.1.4 Centriacinar Emphysema

There are two common forms of emphysema: panacinar and centriacinar. Centriacinar emphysema is preferentially located in the apices of the upper lobes of the lungs, unlike panacinar emphysema which has no regional preference [10]. Dilation of terminal and respiratory bronchioles is also characteristic of centriacinar emphysema, whereas destruction of the alveolar sacs is also included in panacinar emphysema. In severe cases, it is difficult to differentiate between centriacinar and panacinar as centriacinar emphysema tends to spread to other lobes as it progresses [10].

The pathogenesis of emphysema is not fully understood, but one theory is that lysosomal elastase is released from neutrophils in the lung [10]. This enzyme destroys elastin which is important for the structure of the lung. Destruction of this protein would lead to compromised integrity of the alveolar wall. Cigarette smoking is thought to stimulate release of neutrophil enzymes and/or reduce activity of elastase inhibitors [10].

1.1.5 Pulmonary Vascular Alterations in COPD

Pulmonary vascular alterations have been linked with COPD [3, 4, 11-17] leading to increased interest in the pulmonary vasculature as it relates to smoking-associated lung disease. Smoke from cigarettes has been shown to cause local tissue hypoxia damaging small pulmonary arteries [18]. Vessel thickening has been observed in pulmonary arteries of smokers without disease, which has led researchers to believe vascular alteration may

come before the development of emphysematous lung [16, 19, 20]. Barr et al. [12] observed that smokers with greater emphysema on CT scans and more severe airflow obstruction were had impaired left ventricular filling, reduced stroke volume, and lower cardiac output, which may relate to increased pulmonary arterial pressure and vascular alterations related to the progression of COPD [12]. Alford et al. [3] observed increased perfusion heterogeneity in smoking subjects with normal lung function and evidence of minor CAE (assessed by CT). Recently, Iyer et al. [4] showed that increased perfusion heterogeneity was reversible by administering sildenafil.

1.2 Computed Tomography

1.2.1 Quantitative Computed Tomography in the Lung

The development of computed tomography (CT) has allowed for rapid, non-invasive assessment of lung structure and function and the invention of spiral CT allowed volumetric lung imaging to be completed within a single breath-hold [21]. As CT technology further progressed, the number of detector rows (multi-detector row CT, MDCT) increased and subsequently increased the rate of acquisition [22]. Today, a single CT scan of the lungs requires a breath-hold of mere seconds.

MDCT imaging allows for high resolution scans of the lungs, which gives us the opportunity to study lung parenchyma, small airways and small pulmonary vessels. Image segmentation is a crucial part of quantitative computed tomography (QCT). Lung segmentations can be used to compute emphysema index (EI), a metric for the extent of emphysema. EI is computed as the percentage of voxels within the lung less than -950 Hounsfield Units (HU) evaluated on inspiratory scans. Airway segmentations provide a

way to compute airway measurements such as wall/lumen area and wall thickness, which are important in the characterization of asthma and chronic bronchitis [23-25].

1.2.2 Dual Energy Computed Tomography

Dual energy computed tomography has been around almost since the inception of CT imaging [26, 27], but it wasn't until relatively recently that technology advanced enough for it to be used clinically. Presently, there are a few DE techniques commonly utilized by clinical imaging systems: fast kV switching, dual source and dual-layer detector.

Fast kilovoltage (kV) switching is performed with a single source and single detector array. The tube potential is rapidly switched from low (80 kVp) to high energy (140 kVp) during scanning [28]. Tube current is not modulated during scanning, so a single current is set for both tube potentials. Exposure time ratio can be adjusted to improve contrast to noise ratio by increasing exposure of low energy X-ray beam. This technique results in good temporal resolution due to nearly simultaneous acquisition of high and low energy images. It also allows for acquisition of a larger field of view. Spectral overlap is increased however due to a single source for high and low energy x-ray beams. Dual source computed tomography (DSCT) employs two x-ray tubes: a high energy (140-150 kVp) and low energy potential (80-100 kVp) [28]. Beam filtration of the high energy tube and individual tube current adjustments allow for reduced image noise. High energy X-ray beam filtration allows for improved spectral separation. The single source, dual layer detector method consists of a single x-ray source and single detector with two scintillation layers, separated by a filter which separates the beam into high and

low energy spectra [28]. The bottom layer detects high energy x-rays, and the top layer detects low energy x-rays.

1.2.3 DECT Perfusion Blood Volume Imaging

Earlier studies of pulmonary perfusion involved measuring insoluble gases exhaled after being infused in a peripheral vein [29, 30]. This method was known as Multiple Inert Gas Elimination Technique (MIGET), developed by Wagner and colleagues, and could measure whole lung and regional ventilation and perfusion. West et al. showed that blood preferentially distributes to gravitationally dependent lung regions, which vary with body posture. Glenny et al. [31, 32] developed a technique using fluorescent microspheres which were injected into the pulmonary circulation. Measurements of microvascular blood flow could be achieved in resected lung samples using this technique. Schuster et al. developed an in-vivo method to measure perfusion blood flow (PBF) in animal models using PET/CT [33-35] which was later adapted to multi-detector row CT (MDCT). Hoffman and colleagues introduced the use of first pass kinetics-based CT imaging to assess regional pulmonary perfusion [36-38] and this methods was used by Alford et al. [3] for the demonstration that emphysema susceptible smokers with normal pulmonary function tests had an increased perfusion heterogeneity.

PBF imaging is performed with a contrast bolus injection while a section of lung is imaged using single energy MDCT. Regional PBF and mean transit time (MTT) can be measured with this technique. Using this technique, Hoffman et al. [22] observed reduced hypoxic vasoconstriction (HPV) response in areas flooded by saline but not in regions flooded by endotoxin (regions of inflammation). Hoffman et al. postulated that an

inability to block HPV may be related to the development of emphysema in smokers with lung inflammation. Alford et al. used perfusion MDCT to show that smokers with normal lung function and CT evidence of minor centriacinar emphysema had increased perfusion heterogeneity measured by PBF and MTT [3].

Fuld et al. next showed that perfusion blood volume (PBV) imaging can be used as a surrogate for PBF imaging [39]. PBV, assessed via a single slow infusion of contrast agent while spiral scanning using DECT, is a much simpler to implement methodology than a cardiac gated CT scan used to follow a high pressure bolus injection of contrast which must be delivered near the heart. Using this technique, Iyer et al. demonstrated that smokers with normal lung function and CT evidence of minor centriacinar emphysema had increased perfusion heterogeneity measured by PBV coefficient of variation (PBV-CV) which was reversible with sildenafil [4].

DECT perfused blood volume (PBV) imaging is performed by administering iodinated contrast via an intravenous line prior to a dual energy scan. Iodine has a k-edge effect, which drastically increases the attenuation of low energy photons and thus increases the signal in the blood [40] (Figure 2). A test bolus scan is sometimes performed first, which consists of series of single energy, axial CT scans at the level of the left atrium with an iodinated contrast bolus injection. A region of interest is set inside the left atrium and the iodine concentration can be tracked as a function of time. When the iodine concentration peaks or plateaus, we assume it has reached steady state equilibration in the pulmonary circulation [4]. The time between the start of the injection and the peak or plateau is the DECT scanning time offset. To perform DECT PBV imaging, a breath-hold is performed to control for lung volume and contrast infusion will

start with scanning commencing after the time offset. Contrast is continuously injected during the scan to ensure that steady state equilibration is maintained.

Three-material decomposition is the method used to reconstruct PBV images, which acts as a map of iodine/blood distribution in the lungs. PBV reconstruction is achieved by estimating air, soft tissue/blood and iodine volume fractions in each voxel from the differences in attenuation in high and low energy images and known attenuation curves of these materials [41]. The result is a map of the distribution of iodine content in the lungs which is related to the blood flow. PBV reconstructions tend to be noisy, so some smoothing is usually necessary to reduce image noise. In addition, metal artifact from contrast saturated blood near the site of injection may reduce image quality. Third generation DECT systems, such as the Siemens SOMATOM Force, has improved spectral separation and detector sensitivity which may allow for contrast diluted infusions when performing DECT PBV imaging. We explore this idea further in Chapters 3 and 4.

Table 1: Global Initiative for Chronic Obstructive Lung Disease (GOLD) classification of COPD stages. Spirometry measurements are post bronchodilator administration.

Severity	**Stage**	**Spirometry**
No COPD, at risk	0	Normal, with COPD symptoms (i.e. cough, sputum, etc.)
Mild COPD	1	$FEV_1/FVC < 70\%$ & $FEV_1 \geq 80\%$
Moderate COPD	2	$FEV_1/FVC < 70\%$ & $50\% \leq FEV_1 < 80\%$
Severe COPD	3	$FEV_1/FVC < 70\%$ & $30\% \leq FEV_1 < 50\%$
Very Severe COPD	4	$FEV_1/FVC < 70\%$ & $FEV_1 < 30\%$

Figure 1: TLC scan of subject with CT evidence for enlarged airspaces which is characteristic of emphysema in the upper lung lobes.

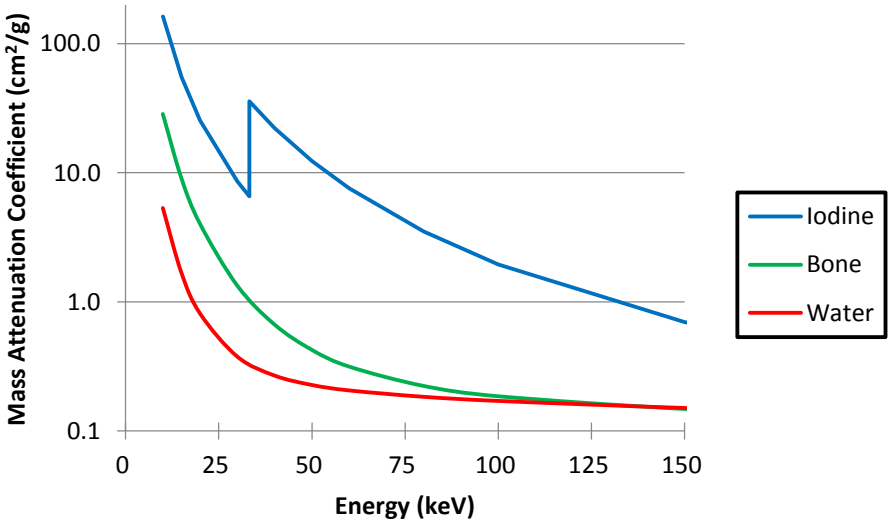

Figure 2: Mass attenuation of Iodine as a function of photon energy. At approximately 30keV a k-edge exists, which drastically increases the signal of iodine relative to other body tissues. This phenomenon allows us to reconstruct PBV images as maps of iodine content in the pulmonary capillary bed.

CHAPTER 2: RAPID EMPHYSEMA PROGRESSORS HAVE ENLARGED CENTRAL PULMONARY ARTERIES RELATED TO DISEASE

2.1 Rationale

As mentioned in Chapter 1, recent studies have supported evidence of a link between COPD and alterations of the pulmonary vasculature [3, 4, 11, 12, 14-17, 42]. The cause of vascular alterations is unclear, but it seems to occur before emphysematous changes in the lung [16, 18, 19]. We believe that downstream constriction related to regional lung inflammation associated with cigarette smoking leads to an inability to maintain perfusion to these regions as a result of failure to block hypoxic vasoconstriction (HPV). HPV is usually blocked in humans in order to maintain perfusion and repair lung inflammation [34, 43]. Pulmonary vascular alteration has been shown to precede emphysema with exposure to cigarette smoke [16, 18, 19]. These findings suggest that pulmonary vascular alteration also alter the HPV response. In previous studies, we have shown, using contrast enhanced computed tomography that smokers with normal lung function and minor centriacinar emphysema (detected via CT) have increased perfusion heterogeneity [3].

In this study, we seek to evaluate the pulmonary arterial dimensions in subjects with and without emphysema progression (assessed by CT) using a custom built graphical user interface to identify and compute arterial cross sectional area [44]. We hypothesize that emphysema progressing subjects will have larger central pulmonary arteries which we believe is related to downstream constriction of small pulmonary arterioles in the presence of smoking associated lung inflammation.

2.2 Methods

2.2.1 Study Cohort

Participants in this study were enrolled in the SubPopulations and InteRmediate Outcome Measures In COPD Study (SPIROMICS) [5]. SPIROMICS is a prospective study of over 3000 subjects classified into four strata: smokers without COPD, mild/moderate COPD, severe COPD and non-smoking controls. Participants were eligible to enroll in SPIROMICS if they were between the ages of 40 and 80 at baseline. Smoking history was limited to $\leq$ 1 pack-year for non-smokers (Stratum 1) and $\geq$ 20 pack-years for current and former smokers (Strata 2 – 4). Participants underwent baseline tests including physical examination, spirometry performed pre- and post-bronchodilator, 6-minute walk test, questionnaires, and thoracic CT scans performed at total lung capacity (TLC, full inspiration) and residual volume (RV, full expiration).

2.2.2 CT Imaging Protocol

Single energy thoracic CT scans were performed with coached breath-hold at TLC and RV without administration of contrast agents at 120 kVp in the supine body posture. X-ray tube current was dependent on BMI, scanner model, and TLC/RV scan [5]. CT scans were conducted within 2 hours post bronchodilator associated with spirometry. Calibration was performed on CT scanners at each site using the COPDGene Lung Phantom [45] prior to subject enrollment and monthly through the duration of the study.

2.2.3 Criteria for Emphysema Progression Groups

Our study evaluated the first 1,855 SPIROMICS participants who completed baseline and one year follow-up (V2) visits. Three groups of subjects were identified from these first 1,855 SPIROMICS subjects based upon their emphysema progression determined from the TLC CT scan pairs (baseline and V2). Emphysema index (EI), calculated as the percent of voxels within the lung with a Hounsfield Unit (HU) less than -950, was used to identify our groups. Rapid progressors (RP) were defined as having a one-year increase in EI greater than 1%. Non progressors (NP) were defined as having a one-year change in EI between -0.5% and +0.5%. The final group contained non-smoking (NS) controls. All groups were restricted to participants with a lung volume difference between baseline and V2 of ±10%. It was assumed that one-year changes in disease status would not cause substantial changes in a participant's TLC. Large changes in lung volume between visits would change regional lung density and interfere with the assessment of actual changes in EI. GOLD 4 and current smoking participants were removed from our analysis due to the fact that very severe COPD influences pulmonary artery pressures and variability in lung inflammation, and thus lung density measures, caused by cigarette smoking which would interfere with accurate assessment of EI. Figure 3 demonstrates how we selected these groups.

2.2.4 Pulmonary Vascular Dimensions

Vessel, lung and lung lobe segmentations were acquired from the Apollo 2.0 workstation (VIDA Diagnostics, Coralville, IA). Peel-core (outer 1.5 cm and remaining core of whole lung) segmentations were processed using the in-house Pulmonary

Analysis Software Suite (PASS). Vessel segmentations, including arteries and veins, were refined to fill in holes and gaps in the central pulmonary vessels and used to measure total pulmonary vascular volume (TPVV) [46]. Whole lung, lobar, core and peel TPVV and %TPVV, TPVV measures in relation to the lung volume for which TPVV was being calculated, were computed. In addition, peel to core TPVV ratio ($\%TPVV_{PC}$) was calculated as the $\%TPVV_{Peel}$ divided by the $\%TPVV_{Core}$.

Labeled airway segmentations and associated airway CSA measurements were acquired from Apollo. A custom-built graphical user interface (GUI), developed within PASS, displayed sagittal, coronal, and transverse views of the CT image and an overlay mask of the target airway segment, previously determined by the user, for which an associated artery segment was sought. An experienced user placed starting and ending points to identify proximal and distal portions of the target artery segment [44].These points of the artery segment coincide with the starting and ending points of the airway segment. The GUI calculates the arterial segment centerline, finds the vessel's edges and subtracts nearby structures: airway walls and neighboring arteries and veins. Computation of the centerline allows oblique arteries segments to be measured. The average cross-sectional area (CSA_{Artery}) and standard deviation of the artery segment are computed and displayed to the user. Inappropriate evaluation of oblique segments can arise from too few slices and can yield an over-estimate of CSA_{Artery}. In order to avoid this, at least eight slices per segment is recommended for these calculations, although very large artery segments may require more slices. Artery segments shorter than this were excluded from our analysis; thus, we include metrics for fewer than 100% of the targeted airway-artery segment pairs, as reported in the results section. CSA_{Artery}

measurements were normalized (CSA_{Norm}) by the associated airway CSA (CSA_{Airway} = lumen area + outer wall area) obtained from Apollo. Defining CSA_{Airway} in this way eliminated biasing the normalization of artery measures by thickened airway walls or mucus lined airway segments, common symptoms in COPD subjects. Arterial segments associated with lower and middle lobe segmental airway branches: RB10, LB10, RB4 and LB4 [44] were evaluated in TLC CT scans for 599 subjects falling into one of the three groups previously discussed: NS, NP and RP. In addition, average CSA_{Norm} was calculated as the average of all four airway-artery pairs per subject.

2.2.5 Statistical Analysis

Participant characteristics and CT measurements from SPIROMICS baseline visits are reported as mean ± standard deviation. One-way analysis of variance (ANOVA) with post-hoc analysis for multiple tests was performed to compare subject characteristics and CT, CSA and TPVV data between NS-NP, NP-RP and RP-NS. Linear regression was performed between average CSA_{Norm} and EI, one-year change in EI, FEV_1/FVC and % predicted FEV_1 among RP participants. EI and one-year change in EI were also regressed in RP participants.

2.3 Results

2.3.1 Participant Characteristics

Vessel dimensions were evaluated in 599 participants: 188 RP, 301 NP and 110 NS. RP and NP participants were approximately the same age (RP: 68 years, NP: 67 years, p=0.1) and had similar history of smoking (RP: 53.8 pack-years, NP: 51.3 pack-

years, p=0.32). RP had more emphysematous lung, larger TLC volume, larger % air volumes, more males, lower BMI, and more severe GOLD status. NS were younger, had smaller TLC volume and more females. A full summary of participant characteristics can be seen in *Table 2*.

2.3.2 TPVV and CSA Measurements

CSA_{Artery} measurements were obtained in 93% of RB10, 90% of LB10, 48% of RB4 and 73% of LB4 associated arteries. CSA_{Airway} was similar among all groups for all target airways, but CSA_{Artery} and CSA_{Norm} varied by group (Table 3). CSA_{Artery} and CSA_{Norm} was significantly larger in RP for arteries associated with RB10 and LB4 airway segments (Table 3), average CSA_{Norm} of all measured artery segments (Figure 6), and CSA_{Norm} of all measured artery segments (Figure 7). %TPVV in the whole lung, peel, core and lobes were all significantly ($p < 0.05$) smaller in RP, but similar in NP and NS (Figure 8). $\%TPVV_{PC}$ was significantly larger in RP than NP and NS (Figure 8).

2.3.3 Association between Vessel Dimensions and Disease Severity/Progression

Average CSA_{Norm} significantly correlated with baseline EI ($R = 0.29$, $p = 7.27e-05$) (Figure 9), FEV_1/FVC ($R = -0.41$, $p = 5.99e-09$) (Figure 10) and % predicted FEV_1 in RP ($R = -0.44$, $p = 5.17e-10$). A significant correlation between baseline EI and one-year change in EI was observed in RP ($R=0.16$, $p = 0.026$) (Figure 11). Average CSA_{Norm} did not correlate with one-year change in EI ($p = 0.97$) among RP participants.

2.4 Discussion

Cross sectional area of central pulmonary arterial segments were evaluated in subjects with rapid and non-progressing emphysema using quantitative volumetric CT imaging. We determined target airways from a previous study [4, 44] which showed good reproducibility for CSA_{Artery} measurement using the algorithm in the custom GUI. Our ability to make a measurement in arteries associated with lower lobe airway segments was greater than 90%, but in the middle lobes it was much lower. Only 48% of RB4 and 73% of LB4 associated arteries could be measured. The reason for this was almost exclusively due to a very common branching pattern we have observed in RB4 and slightly less common branching pattern in LB4. In each case, the parent artery, which we have defined as being associated with our target airway, cannot be measured because there is no artery segment specifically related to the target airway. Instead, the artery one generation previous (grandparent) will branch into many smaller arteries containing RB4/LB4 child associated arteries and often RB5/LB5 parent or child associated arteries. While the GUI is simple to use and the algorithm computes the CSA_{Artery} in a fraction of a second, making these measurements are not trivial. An experienced user is necessary in order to accurately and precisely perform this type of analysis due to aberrant branching patterns of airways and arteries.

We showed that subjects defined as having rapidly progressing emphysema had larger central pulmonary arteries and airway-normalized arteries than subjects with non-progressing emphysema. This finding is consistent with Wells' study of pulmonary artery to aorta diameter ratio (PA:A) in subjects with COPD [17], which showed a relationship between a PA:A ratio greater than 1 and increased prevalence of severe exacerbations

related to COPD. In addition, we also observed smaller $\%TPVV_{Peel}$ and increased $\%TPVV_{Peel}/\%TPVV_{Core}$ in rapidly progressing emphysema subjects which may indicate smaller core venous volumes reflective of increased peripheral arterial resistance. In the Matsuoka et al. study of small pulmonary vessels in COPD subjects [14], a negative correlation was observed between the total area of small pulmonary vessels and extent of emphysema. While Matsuoka et al. findings likely reflected peripheral parenchymal destruction, we believe that our measurements showing a greater TPVV decrease in the lung core reflects the paired loss of venous pressure associated with increased arterial pressure (i.e.: increased central pulmonary arterial cross sectional area at the segmental level). These findings further support our hypothesis that emphysema progression is related to vascular dysfunction and alteration.

In addition to relating these measurements to the extent of emphysema, we also observed a relationship between CSA_{Norm} and disease severity (% predicted FEV_1 and FEV_1/FVC). A relationship was observed between EI and the change in EI suggesting that emphysema progresses at an increased rate as increasing amounts of healthy lung tissue is compromised by disease.

2.5 Summary

In this chapter, we identified subjects from the SPIROMICS cohort as rapid and non-emphysema progressors. A custom built GUI was used to locate and measure the CSA of arteries associated with RB10, LB10, RB4 and LB4 airway segments in these subjects in order to test the hypothesis that emphysema progression is related to vascular dysfunction, specifically increased peripheral arterial resistance related to smoking

associated lung inflammation and disease. The most important finding of this study was that RP subjects had significantly larger airway-normalized arteries compared to NP and NS subjects, which support the hypothesis that emphysema subjects sustain arterial vasoconstriction within inflamed lung regions. In the next chapters we use DECT PBV imaging in order to measure regional perfusion heterogeneity with reduced radiation doses and dilution of the contrast agent, develop protocols for future human studies and evaluate factors influencing our perfusion heterogeneity measurement, PBV coefficient of variation.

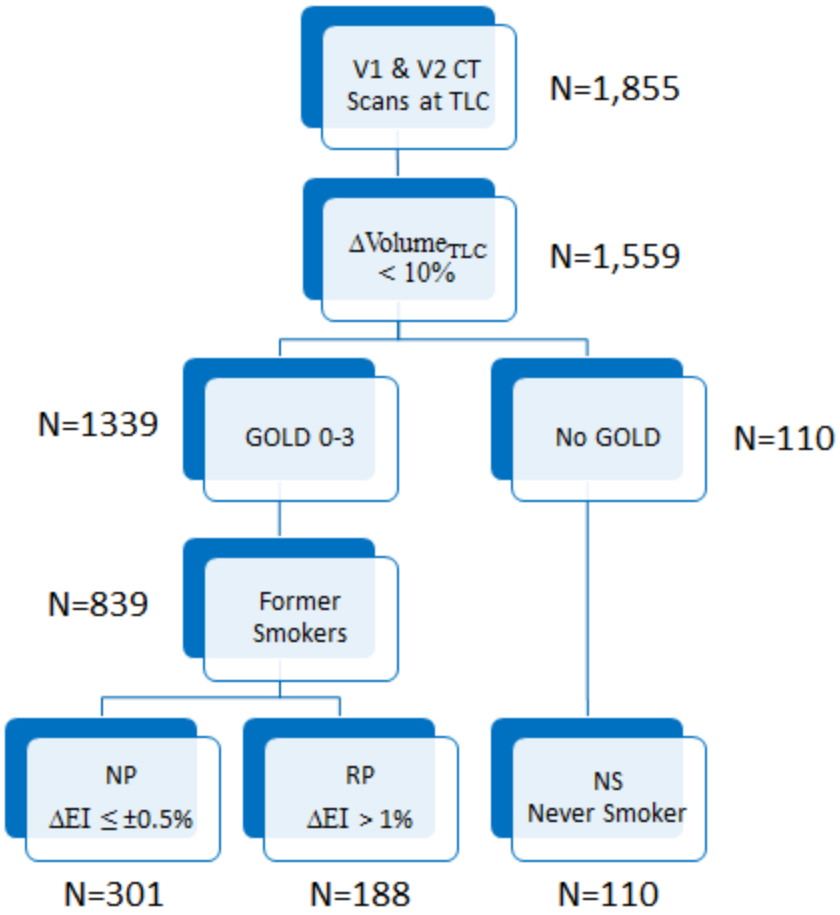

Figure 3: Flow chart of methods for defining the three groups of subjects used in this analysis: RP, NP, and NS.

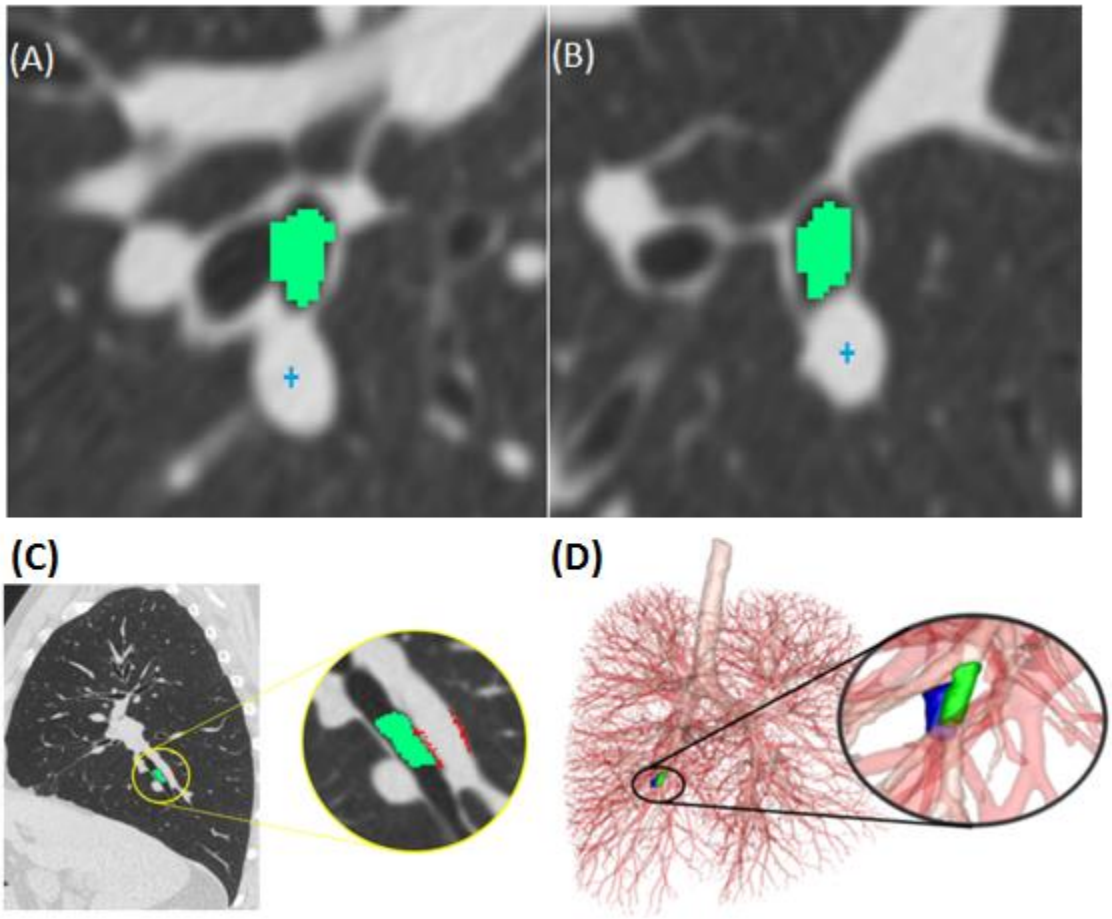

Figure 4: Starting (A) and ending (B) points placed by user to compute the average cross sectional area of the target artery (CSA_{artery}). The artery centerline is computed from these two points and rays are cast to find the edges of the vessel. Neighboring airways and abutting veins and arteries are identified and removed from the CSA_{artery} calculation. Sagittal (C) and 3D rendered (D) views of the labeled airway (green) and artery (red outline in C, blue in D) pair. In most cases, the airway and artery segments are in close proximity and reasonably parallel to one another.

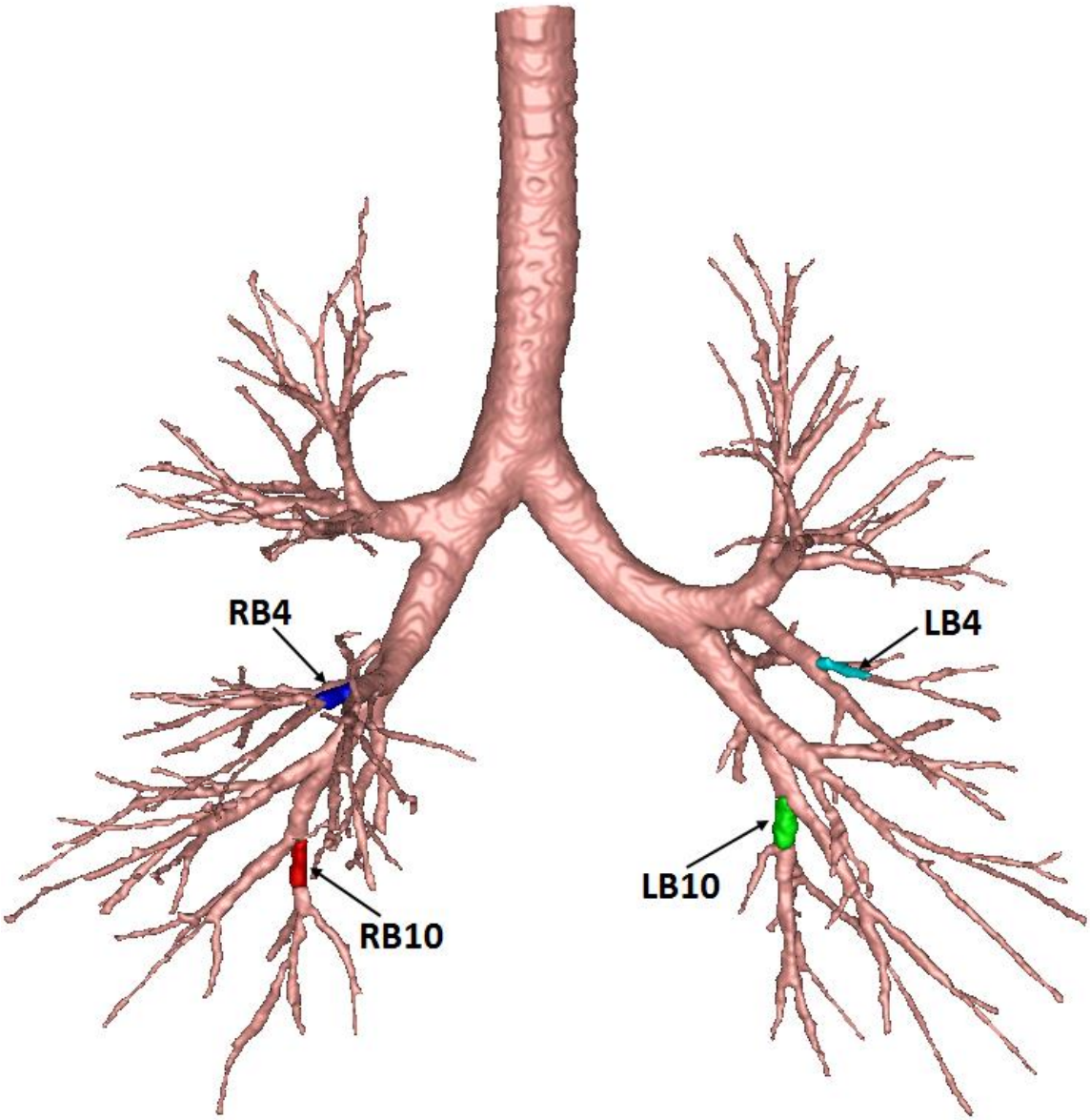

Figure 5: Human airway tree with target airways for our analysis labeled: RB4 (blue), LB4 (cyan), RB10 (red) and LB10 (green). Human airways generally follow the same branching pattern which has led to a standardized labeling system.

Table 2: Subject characteristics for rapid progressors (RP), non progressors (NP) and non-smoking controls (NS). Results are expressed as mean ± standard deviation with the exception of sex (% male) and GOLD status. N, number of subject; TLC, total lung capacity; EI, emphysema index; MLD, mean lung density; BMI, body mass index; FEV_1, forced expiratory volume in 1 second; FVC, forced vital capacity; GOLD, Global initiative for chronic Obstructive Lung Disease. * $p<0.05$ RP vs. NP, $^{\#}$ $p<0.05$ NP vs. NS, $^{\$}$ $p<0.05$ NS vs. RP

Characteristic	**RP**	**NP**	**NS**
N	188	301	110
Δ TLC Volume (%) *$	1.69 ± 4.0	-0.66 ± 4.2	-0.34 ± 4.7
Δ EI (%) *#$	2.45 ± 1.6	0.02 ± 0.3	-0.14 ± 0.5
EI (%) *#$	13.33 ± 10.1	3.86 ± 6.3	1.60 ± 1.7
MLD (HU) *$	-858 ± 19	-829 ± 27	-833 ± 25
Air Volume (L) *#$	5.58 ± 1.2	4.73 ± 1.2	4.47 ± 1.1
Tissue Volume (L) *#$	0.85 ± 0.17	0.88 ± 0.17	0.81 ± 0.14
TLC Volume (L) *#$	6.43 ± 1.4	5.61 ± 1.3	5.28 ± 1.2
Age (years) #$	68 ± 6	67 ± 8	56 ± 10
Sex (male %) *#$	58.5	45.5	35.5
Height (in.) $	67.2 ± 3.8	66.8 ± 4.0	66.2 ± 3.6
Weight (lbs.) *#	174 ± 35.8	189 ± 38.5	176 ± 37.6
BMI (kg/m^2) *#	27.0 ± 4.6	29.7 ± 4.8	28.2 ± 5.0
Smoking Pack Years	53.8 ± 24.7	51.3 ± 28.5	N/A
FEV_1 % Predicted *#$	64.9 ± 24.3	82.2 ± 21.3	103.6 ± 12.2
FVC (L) #$	3.19 ± 1.0	3.19 ± 1.0	3.63 ± 0.9
FEV_1/FVC (%)*#$	48.7 ± 13.5	64.6 ± 13.1	78.9 ± 4.7
GOLD Status:			
GOLD 0	17	146	0
GOLD 1	31	50	0
GOLD 2	78	75	0
GOLD 3	62	30	0

Table 3: Airway, artery and normalized CSA measurements by group. Results are expressed as mean ± standard deviation. Results that significantly differ ($p < 0.05$) from one another are marked as follows: *RP-NP, $^{\#}$NP-NS and $^{\$}$NS-RP.

		Group		
Airway Branch	CSA Measure	NS	NP	RP
RB10	Airway	60.45 ± 14.1	59.33 ± 14.7	58.51 ± 14.0
	Artery **$^{\$}$	41.19 ± 14.5	42.52 ± 14.8	46.80 ± 20.4
	Norm **$^{\$}$	0.693 ± 0.22	0.730 ± 0.22	0.812 ± 0.32
LB10	Airway	66.13 ± 14.8	66.00 ± 17.5	65.33 ± 16.3
	Artery $^{\#\$}$	39.21 ± 12.7	45.43 ± 17.0	47.11 ± 19.1
	Norm $^{\#\$}$	0.614 ± 0.18	0.702 ± 0.23	0.743 ± 0.30
RB4	Airway	43.40 ± 11.0	41.71 ± 11.0	41.57 ± 10.1
	Artery $^{\$}$	22.26 ± 8.1	24.27 ± 7.7	26.13 ± 9.6
	Norm $^{\#\$}$	0.524 ± 0.17	0.603 ± 0.21	0.640 ± 0.21
LB4	Airway	39.67 ± 10.0	41.20 ± 12.1	40.23 ± 13.3
	Artery *$^{\#\$}$	20.50 ± 7.8	24.02 ± 10.5	26.75 ± 11.9
	Norm *$^{\$}$	0.523 ± 0.17	0.590 ± 0.22	0.684 ± 0.26

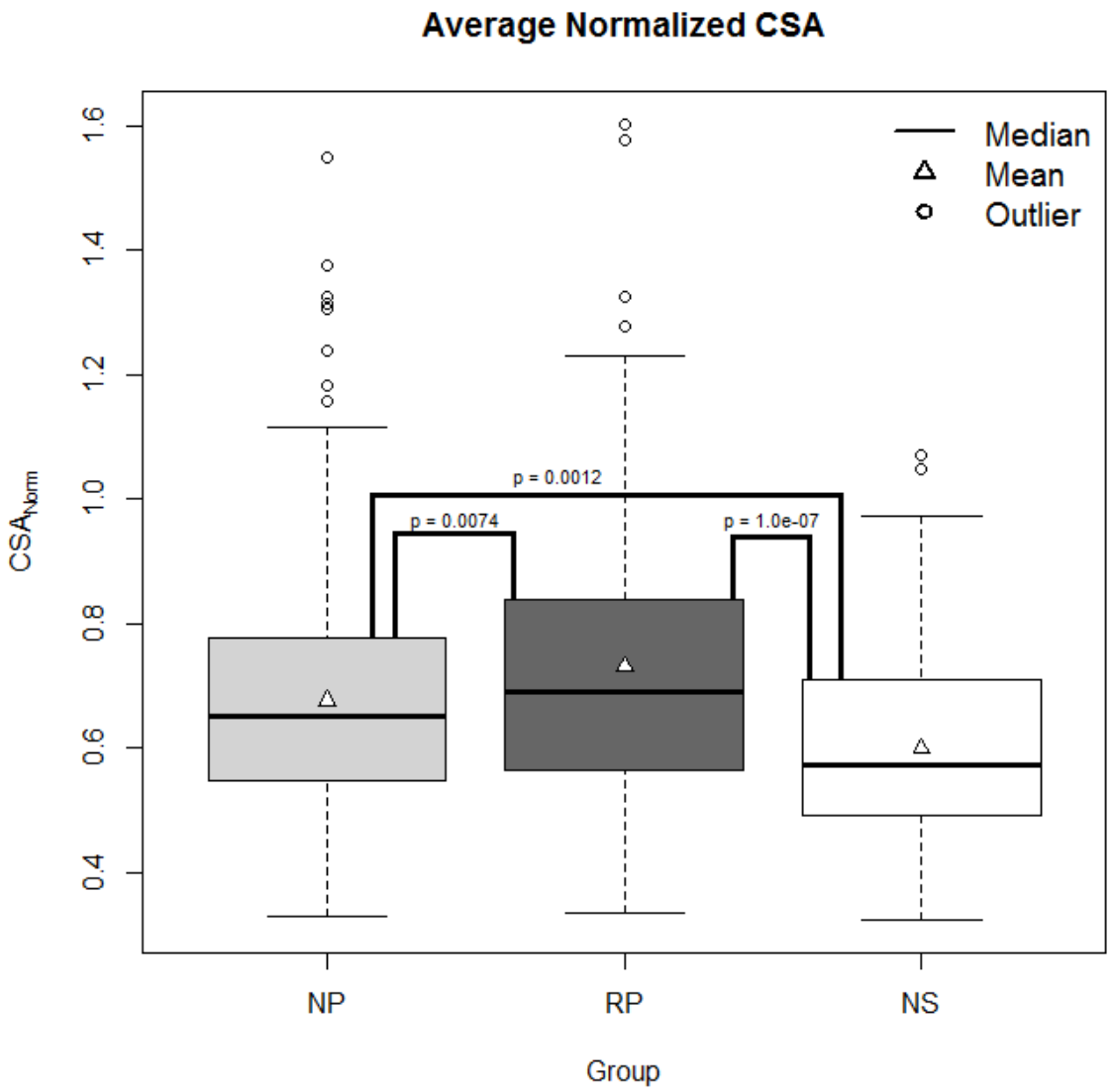

Figure 6: Box plot distribution of average CSA_{norm} in RP, NP, and NS.

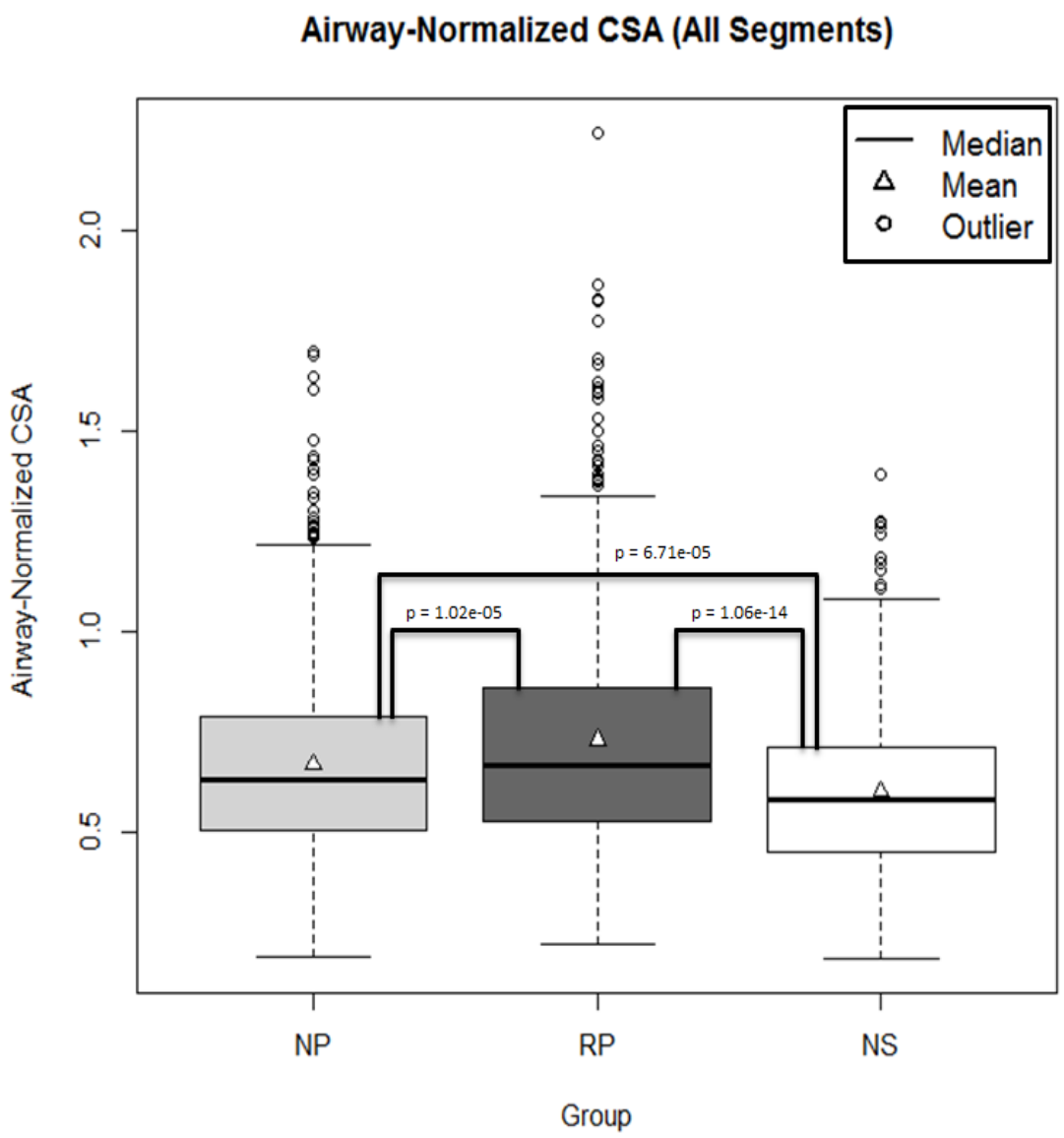

Figure 7: Box plot distribution of all airway associated CSA_{norm} measurements in RP, NP, and NS.

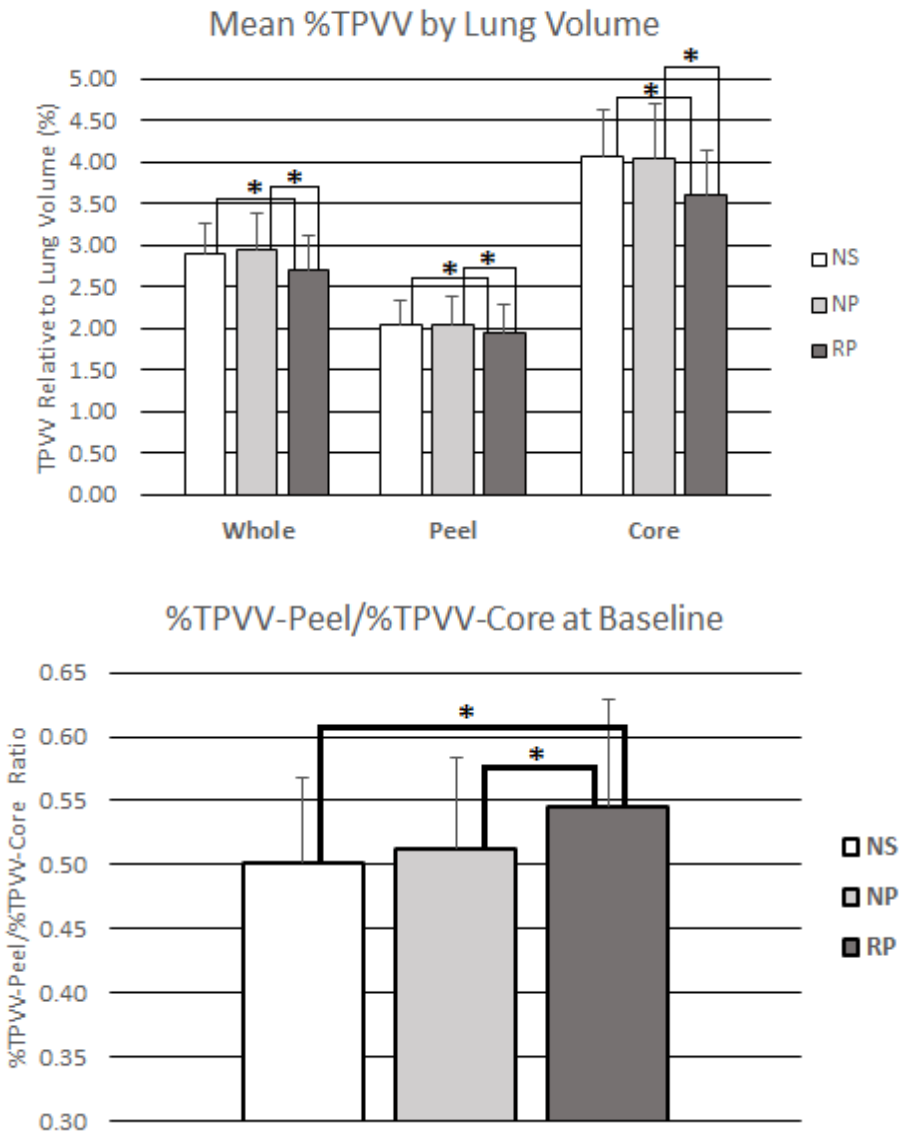

Figure 8: Mean total pulmonary vascular volume relative to associated lung volume (%TPVV) (top) and $\%TPVV_{Peel}/\%TPVV_{Core}$ (bottom) in RP, NP and NS groups.

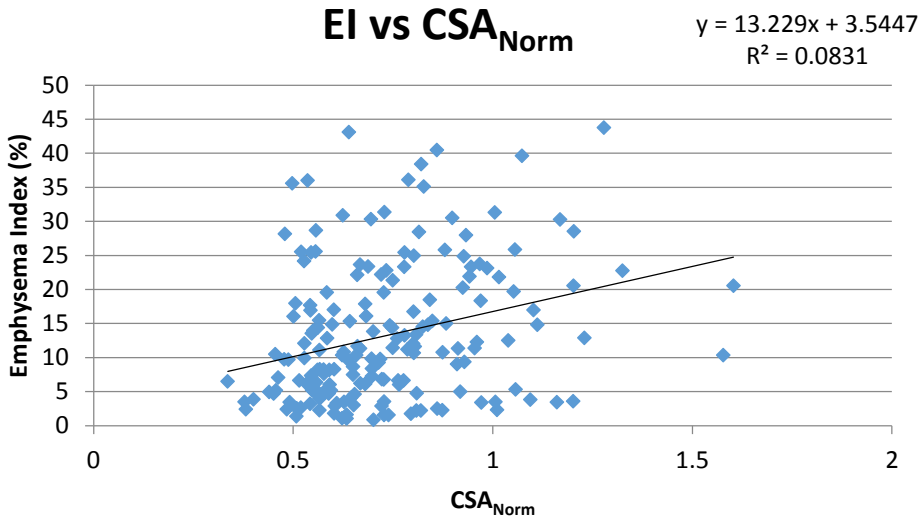

Figure 9: Baseline emphysema index correlated with RB10 associated CSA_{Norm} (top) and LB4 associated CSA_{Norm} (bottom). Both regressions were statistically significant ($p<0.05$).

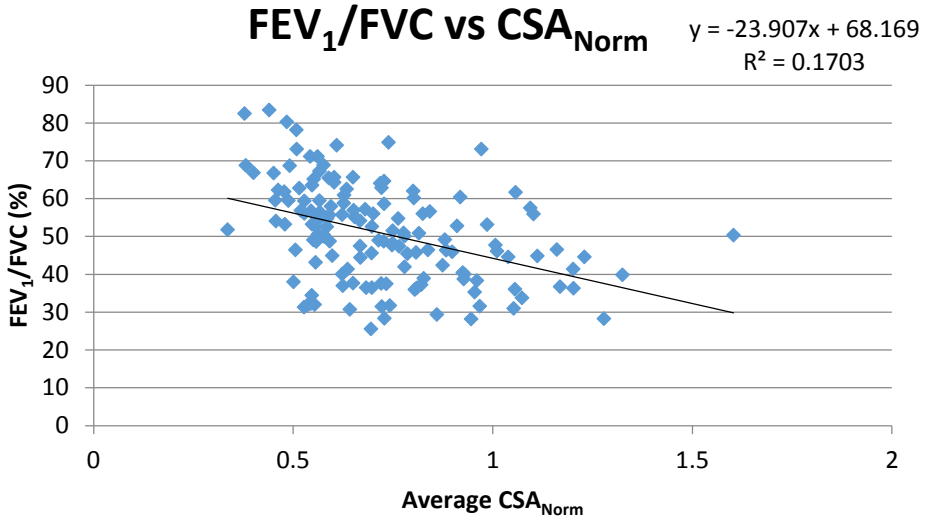

Figure 10: Baseline FEV_1/FVC correlated with RB10 associated CSA_{Norm} (top) and LB4 associated CSA_{Norm} (bottom). Both regressions were statistically significant ($p << 0.001$).

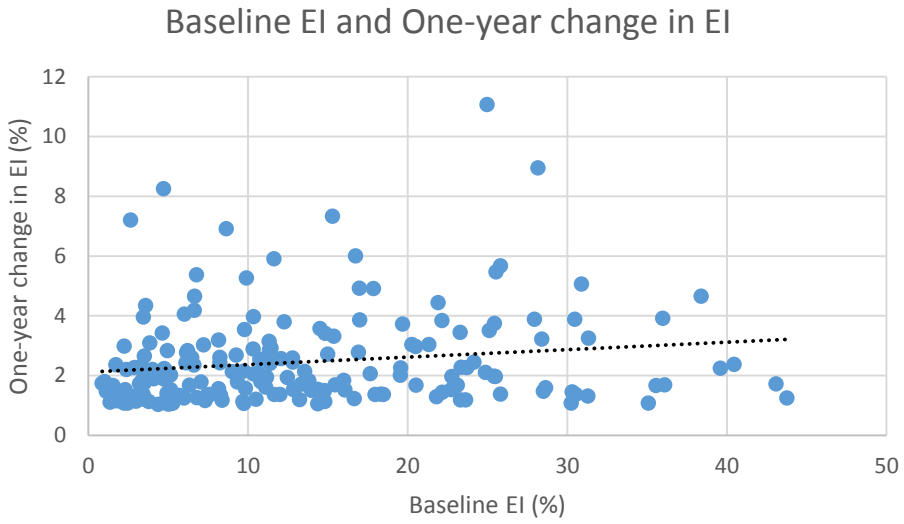

Figure 11: Although weak, a statistically significant ($p<0.05$) relationship was observed between baseline EI and one year change in EI, which suggests emphysema progresses more rapidly as more healthy lung tissue is compromised.

CHAPTER 3: EVALUATING PULMONARY PBV METRICS WITH RADIATION DOSE REDUCTION AND CONTRAST DILUTION IN A LARGE ANIMAL MODEL

3.1 Rationale

Dual energy CT (DECT) perfused blood volume (PBV) imaging is a functional imaging technique that can be used as a surrogate to conventional CT perfusion studies where first pass kinetics approaches requiring cardiac gated axial scanner prove cumbersome to implement [39]. DECT-PBV imaging is gaining traction as a method of measuring perfusion heterogeneity in subjects with COPD [4]. When implemented using a dual source CT scanner (Siemens Definition Flash or SOMOTOM Force) DECT-CT is accomplished without an increase in x-ray dosage since the two components of a single x-ray gun spectra are divided across two x-ray sources. However, it is always a desire to reduce radiation dose as much as possible and to reduce the required dose of a delivered contrast agent. In response, DECT technology continues to improve detector sensitivity and efficiency in an attempt to reduce image noise and subsequently, radiation dose. Emerging iterative reconstruction algorithms serve to further reduce image noise and radiation dose. As methods for reducing image noise and artifacts improve, it is important for researchers to develop imaging protocols to investigate how low we can set radiation dose, so that we may reduce the effect of ionizing radiation on the general population and still get quality image data. The reduction of radiation dose allows for the interjection of a functional scan into an existing non-contrast protocol for the linkage of structure and function and it allows for the use of functional scanning within the context of a longitudinal study.

In this study, we develop a DECT imaging protocol to evaluate the effect of reduced radiation doses on regional PBV metrics in a pig model taking advantage of the increased sensitivity and improved iterative reconstruction methods associated with the Siemens SOMATOM Force CT scanner. The over-riding goal of our study is to find the lowest radiation dose possible along with the lowest concentration of iodine contrast agent for assessing regional pulmonary PBV without subjecting our data to a significant increase in noise.

3.2 Methods

3.2.1 Surgical Protocol

All animal studies were conducted with the approval of the University of Iowa Animal Care and Use Committee. Six swine (40 – 48 kg) were pre-anesthetized with ketamine (1.1mg/kg), xylazine (1.1mg/kg) and telazol (2.2mg/kg) delivered intramuscularly. Anesthesia was delivered via nose cone with 2-3% isoflurane and ventilated with a Harvard large animal mechanical ventilator (source). A peripheral ear vein was accessed with an intravenous (IV) line for saline drip, paralytic agent delivery and emergency drug delivery. A balloon cuffed endotracheal (ET) tube (7-8 G) was used for intubation, prior to tracheostomy. The external jugular vein was isolated, occluded and cannulated with a central IV line for contrast delivery. A tracheostomy was performed and the previous ET tube was replaced to ensure proper sealing and ventilation. Supplemental oxygen was provided during surgery and imaging. Tidal breaths were delivered at 10mL/kg and positive end expiratory pressure of 5 cm H_2O.

Heart rate, temperature, oxygen saturation (SpO_2) and end tidal CO_2 ($ET\text{-}CO_2$) were continuously and recorded every 5-10 minutes during surgery and imaging.

3.2.2 Imaging Protocol

CT imaging was performed with a 3rd generation dual source, dual energy CT scanner from Siemens (SOMATOM Force). High/low energy x-ray tubes were set at 150/80 peak kilo-voltage (kVp) respectively. The high energy x-ray beam utilized tin (Sn) filtration to further narrow the x-ray spectrum so as to increase spectral separation of the two x-ray beams. CARE dose was used for all DECT scans in order to match noise level between the low and the high energy tube over the length of the scan. Reference tube currents ranged from 85 – 318 milli-ampere seconds (mAs) in the high energy tube and 47 – 177 mAs in the low energy tube to create a range of radiation doses to compare dual energy derived perfused blood volume images. Radiation dose, measured as CT dose index volume ($CTDI_{vol}$), ranged from 3.02 – 11.3mGy.

Animals were scanned in the supine body posture to mimic clinical imaging studies and to increase the ventral-dorsal gravitational gradient in PBV, allowing for assessment of our ability to detect this gradient. A water column was added to the expiratory side of the ventilation circuit in order to control mean airway pressure during expiratory breath-holds (positive end expiratory pressure) and for alveolar recruitment. Breath-holds were performed at 15 cmH_2O during all CT image acquisitions so as to further increase the ventral-dorsal gradient being detected (relative to 0 cmH_2O). A test bolus scan was acquired prior to DECT PBV imaging. A 30 mL iodinated contrast bolus was injected via the central IV line (4 cc/s) while a series of single energy (120 kVp)

axial CT scans were acquired at the height of the left atrium. A region of interest (ROI) was placed in the left atrium to compute the transit time for contrast equilibration in the lungs, which was 12 – 14 seconds for all animals. Dual energy scans were then acquired with this contrast injection time delay. Contrast injections were delivered (4 cc/s) with 50%/50% mixture of contrast/saline. High and low radiation doses were paired together during the same breath-hold and contrast infusion in order to minimize the effect of changing physiology over the duration of the animal study. Radiation doses (in mGy) for each animal are shown in Table 4. Breath-holds, including contrast delay and imaging time, were approximately 30 seconds.

3.2.3 DECT Imaging Analysis

DECT images were reconstructed at 0.75/0.5mm thickness/interval using iterative reconstruction (Admire, Siemens). Scanner associated three-material decomposition software (Syngo.Via, Siemens) was used to generate PBV images representing the distribution of iodine in the lungs. PBV samples were taken from the pulmonary artery (PA) in order to normalize the parenchymal PBV ($\%PBV_{PA}$) to purely iodinated blood in the PA. Mixed CT images were computed as 60% of the 80 kVp image and 40% of the 150kVp image in order to create an image with similar noise and contrast as that of a single energy 120 kVp image. Mixed CT images were used to generate lung masks from the PASS. Lung masks were used to remove voxels in the PBV image corresponding to non-parenchymal voxels in the mixed CT image. PBV images were then regionalized into 30x30x40 regions (average region size: 0.2 – 0.4 cm^3) in order to compute $\%PBV_{PA}$ and PBV – coefficient of variation (PBV-CV), a measure of perfusion heterogeneity, within each region. PBV-CV was computed as the standard deviation of iodine concentration

divided by the mean iodine concentration. Regions with fewer than 100 voxels were excluded from the analysis to remove the effect regions with few samples would have on the perfusion metrics. Mean regional $\%PBV_{PA}$ and PBV-CV were computed using valid lung regions. In addition, $\%PBV_{PA}$ and PBV-CV gradients were calculated by averaging regions of the same height (30 samples) from the table in the dorsal to ventral direction. These values were used to evaluate the gravitational effect on PBV metrics across animals as they relate to varying levels of radiation dose.

3.2.4 Statistical Analysis

Regional $\%PBV_{PA}$ and PBV-CV, as well as $\%PBV_{PA}$ and PBV-CV gradients at specific reference $CTDI_{vol}$ were averaged across all animals and expressed as mean ± standard deviation. These values were then compared using one-way ANOVA with post-hoc analysis for multiple comparisons using a significance level of 0.05. In order to simplify the analysis of $\%PBV_{PA}$ and PBV-CV gravitational gradients, the gradients at each target $CTDI_{vol}$ were averaged by region level (1 – 30) from the table, with the first (1 and 2) and last two (29 and 30) regions removed as these areas tend to be noisy and have the fewest samples available. One-way ANOVA with post-hoc analysis for multiple comparisons was then performed to compare average gradients at each target $CTDI_{vol}$. Multiple linear regression was performed to predict PBV-CV from lung volume, actual $CTDI_{vol}$ (mGy), and mean regional PBV signal (HU). Mean parenchymal PBV signal was used in the regression analysis to account for the effect of changes in physiology, possible contrast leaking and the time of contrast infusion.

3.3 Results

Regional %PBV_{PA} did not differ by $CTDI_{vol}$ and ranged from 13 – 14% of PBV_{PA} (Table 5, Table 6). Regional PBV-CV however was dependent on $CTDI_{vol}$ (Table 5, Table 6). Multiple linear regression analysis found iodine signal and actual $CTDI_{vol}$ to be significant predictors of PBV-CV (Table 7). Iodine signal was the most significant feature in the model. Multiple comparison analysis of %PBV_{PA} and PBV-CV gravitational gradients found no significant differences among the $CTDI_{vol}$ levels used in this analysis (Figure 12, Figure 13). Regional %PBV_{PA} did not differ by radiation dose and the average regional PBV-CV at higher doses (11.3 and 7.47 mGy) and lower doses (5.32 and 3.02 mGy) were similar.

3.4 Discussion

The reduction of dose between 11.3 and 7.47 mGy while maintaining a similar regional PBV-CV represents a $CTDI_{vol}$ reduction of 34% without compromising our PBV heterogeneity measurement. On this particular scanner, with pigs of this size, this radiation dose is approximately 3.5 mSv. In addition, although PBV-CV was significantly larger in lower radiation dose scans, visually, the image quality was still very good in the low dose PBV images and the shifts in the ventral-dorsal PBV slopes were parallel. Average %PBV_{PA} and PBV-CV gradients at each $CTDI_{vol}$ pair did not differ from one another. This finding suggests that even with variable radiation dose, we can still measure the gravitational effects on PBV metrics with accuracy.

The multiple linear regression analysis predicting regional PBV-CV from actual $CTDI_{vol}$, iodine signal (PBV) and FRC volume found PBV and $CTDI_{vol}$ to be significant

predictors, but iodine signal to be the most important feature in the model. Iodine signal is dependent on numerous factors including the concentration of the contrast injection, the time delay from contrast injection and CT scan, and physiological factors such as the cardiac output. Increased concentration of contrast injection will increase the iodine signal in the blood and thus reduce the PBV-CV measurement as it is a ratio of the standard deviation of iodine signal to the mean of the iodine signal. The longer the time delay between contrast injection and commencement of CT scanning the more iodine signal there is in the blood until equilibration. This effect should be minimized as we perform test bolus scans to determine time to equilibration, however, it's possible that iodine leak into extravascular spaces could occur during scanning which would further increase iodine signal in the parenchyma. Lastly, changes in cardiac output either from changes in heart rate or ejection volume could change the iodine signal during a study. It is unlikely that these changes would be noticeable within a single breath-hold, but more likely this effect could be noticed over the duration of an imaging study.

3.5 Summary

In this study, we attempted to develop a low radiation dose, low contrast DECT PBV imaging protocol in order to implement in future human DECT PBV scans. Radiation doses ranged from 3.02 – 11.3 mGy (reference $CTDI_{vol}$) and a 50/50 contrast/saline infusion was injected with a time delay of ~12 seconds and for the duration of the scan.

PBV images were split into 30x30x40 regions and $\%PBV_{PA}$ and PBV-CV were computed within each region. Mean regional $\%PBV_{PA}$ and PBV-CV were computed by

averaging all valid lung regions. PBV metrics from the same reference $CTDI_{vol}$ were averaged across animals and compared. A multiple linear regression model was constructed to measure the effect of radiation dose, iodine signal (PBV) and lung volume on PBV-CV. PBV-CV did not significantly differ among the two highest radiation doses nor the two lowest, but did differ between the high and low radiation doses. Radiation dose did have a significant effect on PBV-CV in the regression model, but iodine signal still remained the more important factor in determining PBV-CV. This finding suggests that factors such as iodine concentration and contrast injection time offset as well as physiological factors such as cardiac output and regional perfusion are more important in the measurement of PBV heterogeneity.

The results of this study still suggest we can reduce radiation dose by approximately 34% and still get very comparable results of PBV heterogeneity. This study is important in the development of low radiation dose protocols as CT, especially DECT PBV, imaging become more popular in clinically and in research studies. The reduction of iodine in this study was also important as it could potentially lead to DECT PBV imaging protocols for subjects with impaired renal function. In the next chapter, we implement a reduced iodine concentration injection in subjects undergoing DECT PBV imaging.

Table 4: Radiation doses used during paired CT scans within a single breath-hold for each animal study. **Timing of test bolus was incorrect, thus data from these scans was not used in our analysis.*

Animal #	**Dose 1 (mGy)**	**Dose 2 (mGy)**	**Dose 3 (mGy)**
1	11.3	7.47	N/A
2	11.3*	5.32	11.3
3	11.3	5.32	11.3
4	7.47	5.32	3.02
5	7.47	5.32	3.02
6	7.47	5.32	3.02

Table 5: Average regional PBV-CV and $\%PBV_{PA}$ values by target $CTDI_{vol}$. Values are reported as mean ± standard deviation. Statistical differences are noted in Table 6.

Ref $CTDI_{vol}$	**PBV-CV**	**$\%PBV_{PA}$**
11.3 mGy	0.274 ± 0.03	0.131 ± 0.02
7.47 mGy	0.291 ± 0.04	0.135 ± 0.02
5.32 mGy	0.320 ± 0.03	0.135 ± 0.03
3.02 mGy	0.331 ± 0.02	0.140 ± 0.02

Table 6: Summary of one-way ANOVA with post-hoc analysis for multiple comparisons of $\%PBV_{PA}$ and PBV-CV by target radiation dose. $\%PBV_{PA}$ did not differ across radiation doses, unlike PBV-CV.

Statistical Test	**PBV-CV**	**$\%PBV_{PA}$**
7.47 mGy – 11.3 mGy	p = 0.62	p = 0.98
5.32 mGy – 11.3 mGy	p = 0.005	p = 0.98
3.02 mGy – 11.3 mGy	p = 0.002	p = 0.84
5.32 mGy – 7.47 mGy	p = 0.124	p = 0.99
3.02 mGy – 7.47 mGy	p = 0.04	p = 0.97
3.02 mGy – 5.32 mGy	p = 0.85	p = 0.95

Table 7: Summary of multiple linear regression analysis predicting regional PBV-CV from iodine signal (PBV) and $CTDI_{vol}$. PBV was the most significant predictor of PBV-CV.

Variable	**Estimate**	**Std. Error**	**T-value**	**p-value**
Intercept	0.582	0.018	32.02	<<0.001
PBV (HU)	-0.0041	0.0003	-13.41	<<0.001
$CTDI_{vol}$ (mGy)	-0.0066	0.0007	-9.535	<<0.001
$R_{adj}^2 = 0.853$, p <2.2e-16				

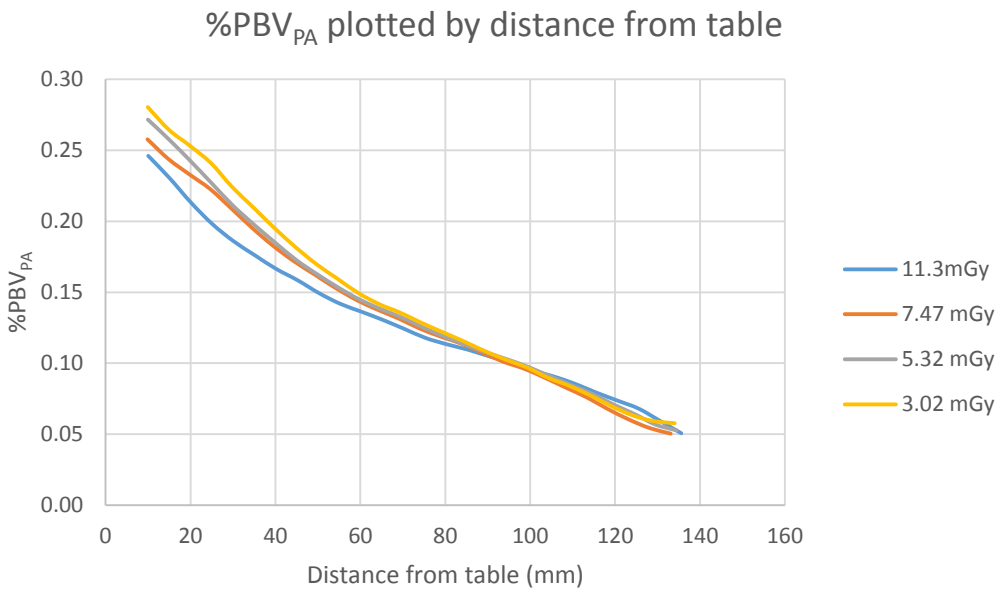

Figure 12: Gravitational effect on %PBV$_{PA}$ across radiation doses. No significant differences were observed. %PBV$_{PA}$ decreases as we travel up from the table from dorsal to ventral in a supine subject.

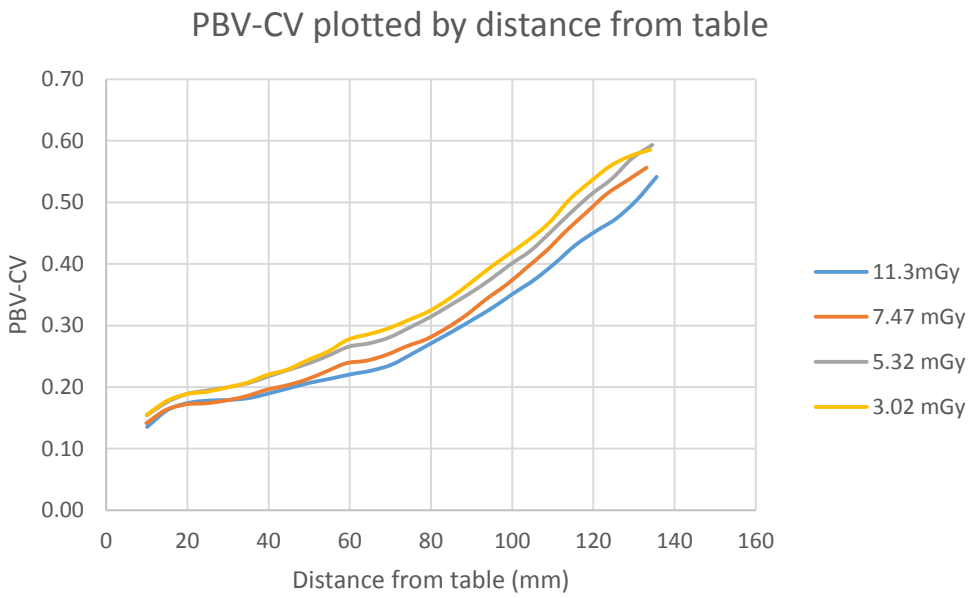

Figure 13: Gravitational effect on PBV heterogeneity across radiation doses. Although mean regional PBV-CV differed among radiation doses, gravitational gradients were similar. PBV-CV increases as we travel up from the table from dorsal to ventral.

CHAPTER 4: ASSESSMENT OF FACTORS AFFECTING DECT-DERIVED PULMONARY PBV IN A MULTI-SITE STUDY COHORT

4.1 Rationale

Quantitative computed tomography (QCT) is a powerful tool that is increasingly being used to study lung disease [5, 45, 47]. Single energy volumetric QCT has been used in conjunction with image processing techniques in order to calculate airway, vessel and lung density measurements [13, 23, 48, 49]. The development of dual energy CT (DECT) technologies has given researchers the opportunity to use CT to study lung structure and function by using two X-ray energy potentials to discriminate between materials. DECT technology can be used for a number of applications including lung ventilation and perfusion [4, 39, 50-53].

DECT performed with administration of a contrast agent can allow a clinician or researcher to study regional lung ventilation [50, 51, 53] or regional pulmonary perfused blood volume (PBV) [39, 52, 53] using three-material decomposition. Three-material decomposition is used to compute the concentration/enhancement of iodine for perfusion or Xenon/Krypton for ventilation. In the case of PBV imaging, iodine content in the pulmonary capillary bed is computed by estimating air, soft tissue/blood and iodine volume fractions in each voxel from the differences in attenuation in high and low energy images and known attenuation curves of these materials. This technique generates PBV images representing the distribution of iodine in the lung and can be reported as either enhancement (HU) or concentration (mg/ml) of iodine.

Pulmonary PBV images can be used to measure the regional distribution of PBV which can be used as a surrogate to perfused blood flow [39]. In addition, regional PBV coefficient of variation (PBV-CV) can be calculated, which is a measure of PBV heterogeneity. A number of diseases are known to result in heterogeneous distribution of blood flow: pulmonary embolism and chronic obstructive pulmonary disease [3, 4, 52]. It was demonstrated that smokers with normal lung function who were characterized (by visual inspection of total lung capacity CT) as emphysema susceptible had increased PBV heterogeneity which was reversible with sildenafil [4]. In this study, we aim to study what effect, if any, that subject and scanner specific factors have on PBV heterogeneity by comparing DE derived pulmonary PBV images acquired from three scanners: Siemens SOMATOM Definition Flash (DSCT), Siemens SOMATOM Force (DSCT) and GE Discovery 750 HD (fast kV switching).

4.2 Methods

4.2.1 Study Cohort

88 subjects underwent contrast enhanced DECT PBV imaging. 71 of these participants were GOLD 0 – 1 smokers recruited from the SPIROMICS [5] cohort (University of Michigan, University of Iowa and The Johns Hopkins University). The remaining 17 subjects were participants in the IRB approved Hypoxic Pulmonary Vasoconstriction [4] study which recruited current smokers with normal lung function from the COPDGene [45] and SPIROMICS [5] cohorts.

4.2.2 DECT Imaging

Subjects were scanned in the supine body posture on one of three DECT scanners: Siemens SOMATOM Definition Flash (128-slice), Siemens SOMATOM Force (192-slice), and General Electric (GE) Discovery 750 HD (128-slice). The DECT scanning protocol for subjects scanned on the Force and GE systems included a coached breath-hold at functional residual capacity (FRC) along with an iodinated contrast (Isovue 370 mg/ml, bracco) injection (4 cc/s) via peripheral vein. Contrast injection was initiated 17 seconds (32) prior to CT scan and persisted through the duration of the scan. Scanning protocol for subjects scanned on the Flash system included 1) 30-ml contrast bolus to determine scanning and contrast injection time offset and 2) a contrast enhanced (continuous 4 cc/s injection) DECT PBV scan at FRC using the offset measured in the test bolus scan [4].

High/low energy potentials were 140/80 kVp on GE and Flash systems and 150/80 kVp on the Force system (Figure 14). Flash and Force systems included tin (Sn) filtration of the high energy X-ray beam. GE and Flash groups were injected with 100% iodinated contrast; the Force group was injected with a mixture of 50%/50% iodinated contrast and saline with the exception of two subjects who were injected with 100% contrast. Additional scanner and reconstruction parameters are listed in Table 8. All subjects were imaged in a spiral mode covering the full apex to base extent of the lungs.

4.2.3 DECT Imaging Analysis

PBV images were created with scanner-associated three-material decomposition software (Figure 15). Mixed CT images were acquired by computing a weighted average

of the high and low energy images in order to achieve similar noise levels to a CT image acquired at 120kVp. Lung masks were acquired from mixed CT images in the Pulmonary Analysis Software Suite (PASS), eroded 1 voxel to reduce edge effects from neighboring ribs, heart and blood vessels and had vessels and airways removed using in-house software. The most recent total lung capacity (TLC) scan available at the time of analysis was registered to the mixed CT image. Image registration was performed using a mass preserving non-rigid B-spline registration technique [54, 55]. Deformed TLC images were used to identify emphysematous lung voxels with a threshold of -950 HU. Regions of interest in the pulmonary artery (PA) were acquired from the PBV image and used to compute PBV relative to the PA ($\%PBV_{PA}$).

4.2.4 PBV Regional Analysis

Lung masks were used to extract parenchymal PBV from the PBV image. PBV images were normalized to the PBV measured in the PA to account for differences in subjects and contrast injection concentration. PBV images were regionalized into 30x30x40 regions (average region volume: 0.3 – 0.6 cm^3) and 7.7 mm x 7.7mm x 7.7 mm (fixed region volume: 0.456 cm^3) regions. Fixed region volume was selected based on the average region size from the 30x30x40 method and was approximately 0.456 cm^3 as voxel spacing differed among all subjects. Mean $\%PBV_{PA}$ and PBV-coefficient of variation (PBV-CV), a measure of perfusion heterogeneity, were calculated in each region. PBV thresholding with mixed CT and warped TLC images were compared. In each case, PBV voxels corresponding to mixed CT or warped TLC image voxels outside the range -200HU to -950HU were removed. In the case of the mixed CT image, this was done in order to remove any remaining pockets of air or airways. In the case of the

warped TLC image, this was done in order to remove emphysematous lung voxels. In addition, the percent of voxels <-950 HU, emphysema index (EI), was computed within each region. Any region with greater than 5% EI was removed. Regions with fewer than 100 lung voxels were excluded in order to remove the effect of small regions on $\%PBV_{PA}$ and PBV-CV. Apical regions, defined as the upper 25% of the lung regions, of the lungs were removed due to image artifact from the site of contrast injection in the subclavian vein. Finally, mean regional $\%PBV_{PA}$ and PBV-CV were computed using valid lung regions (see Figure 16 for summary of this analysis).

4.2.5 Statistical Analysis

Subject characteristics, volumetric CT data, $\%PBV_{PA}$ and PBV-CV are reported as mean ± standard deviation. One-way analysis of variance with Tukey's honest significant difference (HSD) test was used to compare continuous data between the three CT scanner groups as well as regional $\%PBV_{PA}$ and PBV-CV. Paired t-tests were used to compare regional $\%PBV_{PA}$ and PBV-CV from the four regional analysis methods within each group. Multiple linear regression models with step-wise selection (R Statistical Software) predicting PBV-CV with subject characteristics, CT data, iodine signal (PBV) and scanner type was constructed to evaluate the importance of these features in the prediction of perfusion heterogeneity and to evaluate the repeatability of DECT PBV imaging on different models of CT scanners and different DECT techniques. PBV-CV from four regional analysis methods was used in the models: 30x30x40 non-warped, 30x30x40 warped, fixed region size non-warped and fixed region size warped.

4.3 Results

4.3.1 Subject Characteristics

We collected DE PBV images for 88 subjects, but excluded eight due to either low cardiac output (reducing PBV signal) or excessive image noise and motion for a total of 80 subjects. The time between the most recent TLC scan and DE PBV scan ranged from same day acquisition to 2 years (mean: 6 months). A TLC scan from two years ago was used for one subject because of poor image quality in the most recent TLC scan. Only eight subjects had TLC scans older than 15 months.

GE subjects were older, had a higher percentage of males, higher EI, and lower FEV_1/FVC. Body mass index (BMI), smoking history and % predicted FEV_1 were similar in GE and Force subjects. FRC volume was similar in all three groups. Flash and Force groups had similar percentage of male subjects and FEV_1/FVC. Flash subjects had very little emphysema, shorter smoking history and larger % predicted FEV_1 (Table 9).

4.3.2 Perfused Blood Volume Derived Metrics

Mean regional $\%PBV_{PA}$ was similar among all groups (~16-20% of PA), but PBV-CV was higher in Force (average: ~0.45 – 0.46) and GE (average: ~0.55 – 0.61) subjects (Table 10, Figure 17). Regional $\%PBV_{PA}$ and PBV-CV did not differ between warped and non-warped PBV images in Force and Flash subjects, but was significantly ($p < 0.05$) higher in non-warped images in GE subjects (Figure 18, Figure 19).

All four multiple linear regression models found scanner type, iodine signal (PBV), BMI and sex to be important predictors of PBV-CV. Both warped models also

included % predicted FEV_1 found to be an important predictor (Table 11, Table 12). Imaging with Siemens CT systems reduced PBV-CV as did increased iodine signal, while PBV-CV was increased in subjects who were male and had increased BMI. Higher % predicted FEV_1 also reduced PBV-CV in warped PBV images. Scanner type was the most significant feature in all models. Estimates of Flash and Force system coefficients in the model were similar.

4.4 Discussion

In this study, we use dual energy computed tomography to map PBV in normal and GOLD 0-1 smoking subjects. We used image registration to warp a recent TLC CT scan to the DE PBV scan in order to remove emphysematous lung regions. Emphysematous lung regions have little to no perfusion, which would affect the measurement of $\%PBV_{PA}$ and PBV-CV. The $\%PBV_{PA}$ values are similar to those found in the Iyer et al. study of perfusion blood volume in normal smoking subjects [4]. The PBV-CV values were also similar to those in the Iyer et al. study; however the PBV-CV values from the GE group were closer to those in the Alford et al. study of perfusion blood flow [3].

In addition to comparing PBV metrics between groups, we warped a non-contrast TLC scan to the DECT-PBV scan in order to remove emphysematous regions from our assessment of PBV and PBV-CV. This was done with the goal of removing the effect that emphysematous lung regions might have on perfusion heterogeneity. Removal of the emphysematous regions had little effect on subjects scanned on Siemens systems since these subjects had little emphysema, especially the subjects scanned on the Definition Flash as they were subjects with normal pulmonary function tests. However, elimination

of emphysematous regions significantly reduced PBV-CV in GE subjects (Figure 20). GE subjects had more emphysema than either of the other groups.

Multi linear regression models were constructed to predict regional PBV-CV from subject sex, age, BMI, smoking pack-years, EI_{-950HU}, % predicted FEV_1, FEV_1/FVC, iodine concentration, and FRC volume. The models found BMI, sex, % predicted FEV_1, iodine signal in the pulmonary artery and scanner model to be important predictors of PBV-CV. The effect of BMI is likely related to increased image noise. Iodine signal is related to the concentration of iodine used in contrast injection as well as the cardiac output (CO) of the subject. After accounting for differences in BMI, sex, % predicted FEV_1 and iodine signal, the CT system used for scanning remained the most significant contributor to PBV heterogeneity. Flash and Force systems had similar estimates of PBV-CV in the regression models. Thus, the differences among other predictors, particularly iodine signal, can account for the difference seen in PBV-CV between the subject groups studied on the two Siemens scanners. These findings also suggest that images acquired with the GE system are inherently noisier than images from the two Siemens systems. We believe this is a result of the dual energy, fast kV switching, technique used by the GE system.

We believe increased image noise from the fast kV switching technique is the most likely explanation for the increased PBV heterogeneity. Unlike DSCT systems, the high energy X-ray beam cannot be filtered on the GE system which increases image noise. In addition, a single tube current is set and cannot be modulated during scanning. Tube current must be decreased in order to keep radiation dose low, which also increases image noise. Emerging iterative reconstruction methods may serve to better reduce noise

in these images. These are important findings as researchers begin using DECT to assess and quantify regional ventilation and perfusion heterogeneity in patients with COPD. When comparing DECT PBV signals between scanners, scanner characteristics must be taken into account.

4.5 Summary

In this study, we used DECT PBV imaging to analyze PBV-CV, a surrogate for perfusion heterogeneity, in a cohort of subjects with none to mild lung disease. Subjects were imaged on one of three CT scanners: Siemens Flash, Siemens Force and GE Discovery 750 HD which utilized two methods to perform DECT: dual source and fast kV switching. Regional measurements of PBV and PBV-CV were made by splitting the PBV image by a fixed number of regions (30x30x40 voxel regions; average size = 0.3 – 0.6 cm^3) and fixed isotropic region size (target size = ~0.456 cm^3; range: 0.41 – 0.48 cm^3) in order to reduce image noise from PBV reconstruction and measure perfusion heterogeneity in healthy lung regions.

The most important finding in this study was that perfusion heterogeneity is dependent on patient BMI, sex, iodine signal and scanner model with the latter being the most significant determinant for inter-subject variation. This finding suggests that differences in the technique utilized by scanners from different manufacturers must be accounted for when performing DECT-PBV imaging in a multi-center study.

Table 8: Dual energy computed tomography scanning parameters in the three DECT scanners used in this study.

CT Scanner Make and Model	**Siemens SOMATOM Definition Flash**	**Siemens SOMATOM Force**	**GE Discovery 750 HD**
DE Method	Dual Source	Dual Source	Fast kV Switching
Low/High Tube Voltages	80/140Sn kVp	80/150Sn kVp	80/140 kVp
Radiation Dose (mGy)	11.41	10.11	12.28
Slice Thickness (mm)	0.75	0.75	0.625

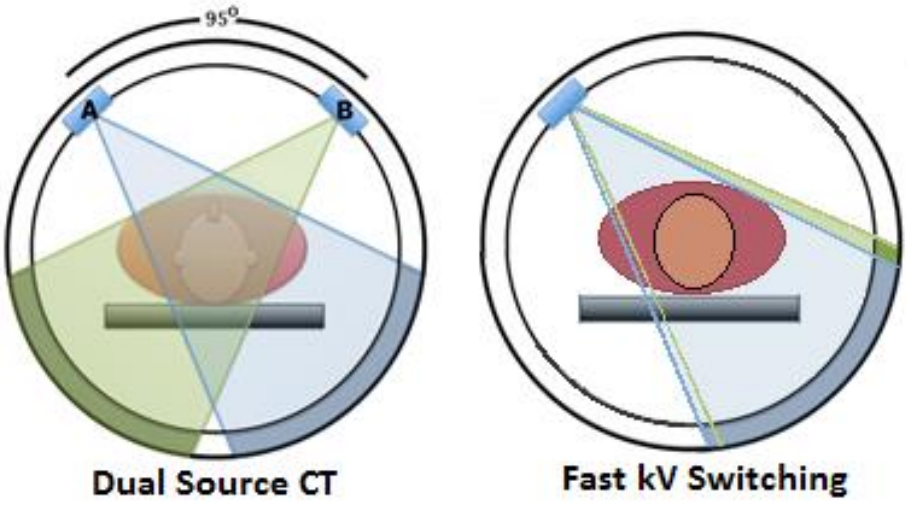

Figure 14: Dual source and fast kV switching dual energy technique diagrams. Dual source is performed with two X-ray sources: low energy (blue) and high energy (green). Fast kV switching is performed by rapidly alternating between low (blue) and high (green) energy beams from a single source.

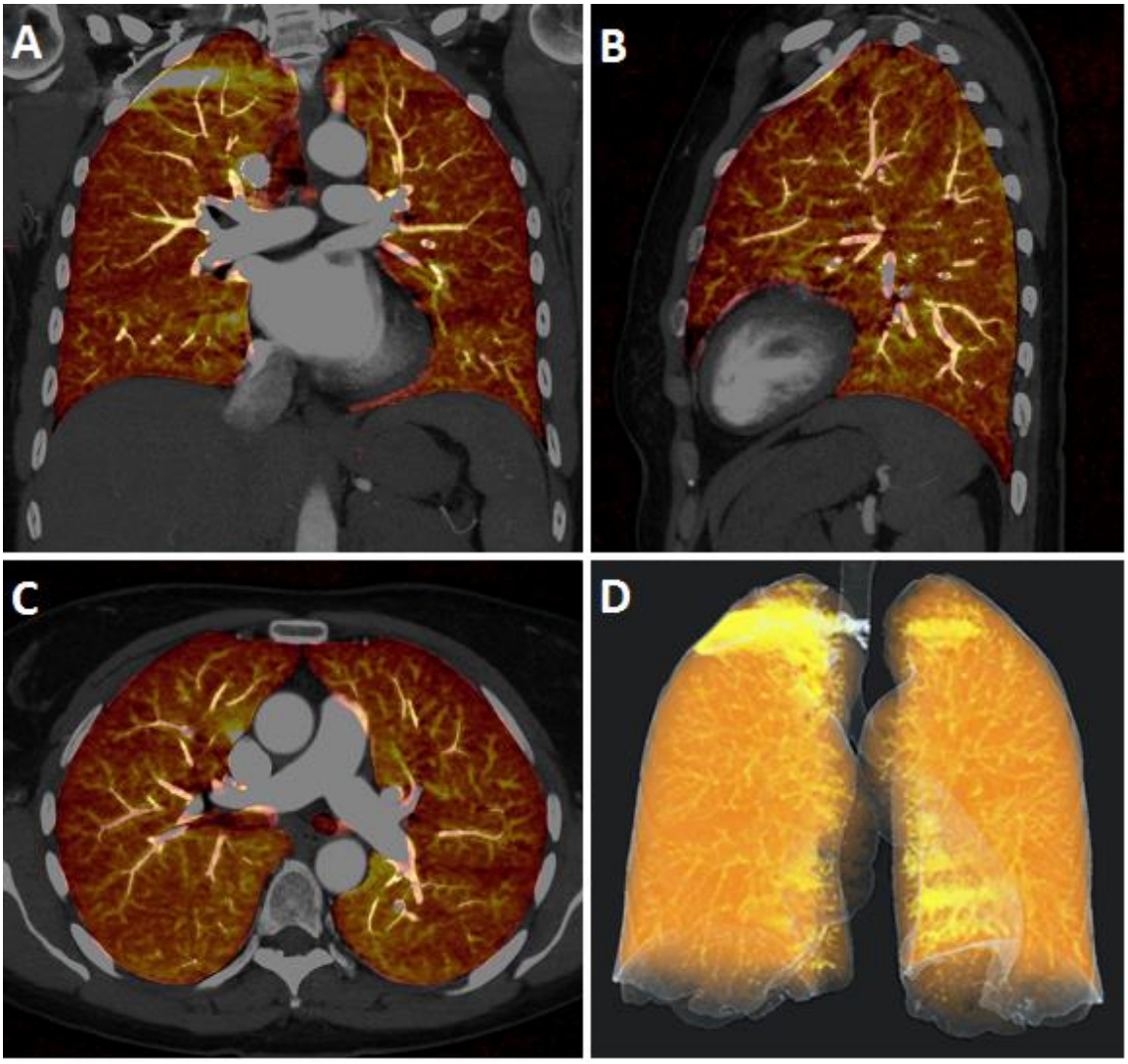

Figure 15: Perfused blood volume image acquired from three-material decomposition software (Syngo.Via, Siemens). Coronal (A), sagittal (B), transverse (C) and 3D (D) views of reconstructed PBV image. Some metal artifact can be seen from the contrast enhanced subclavian vein, which is the site of contrast infusion in the apex of the right lung (A, D). PBV samples from the pulmonary artery (PA) allow us to compute PBV relative to the PA ($\%PBV_{PA}$).

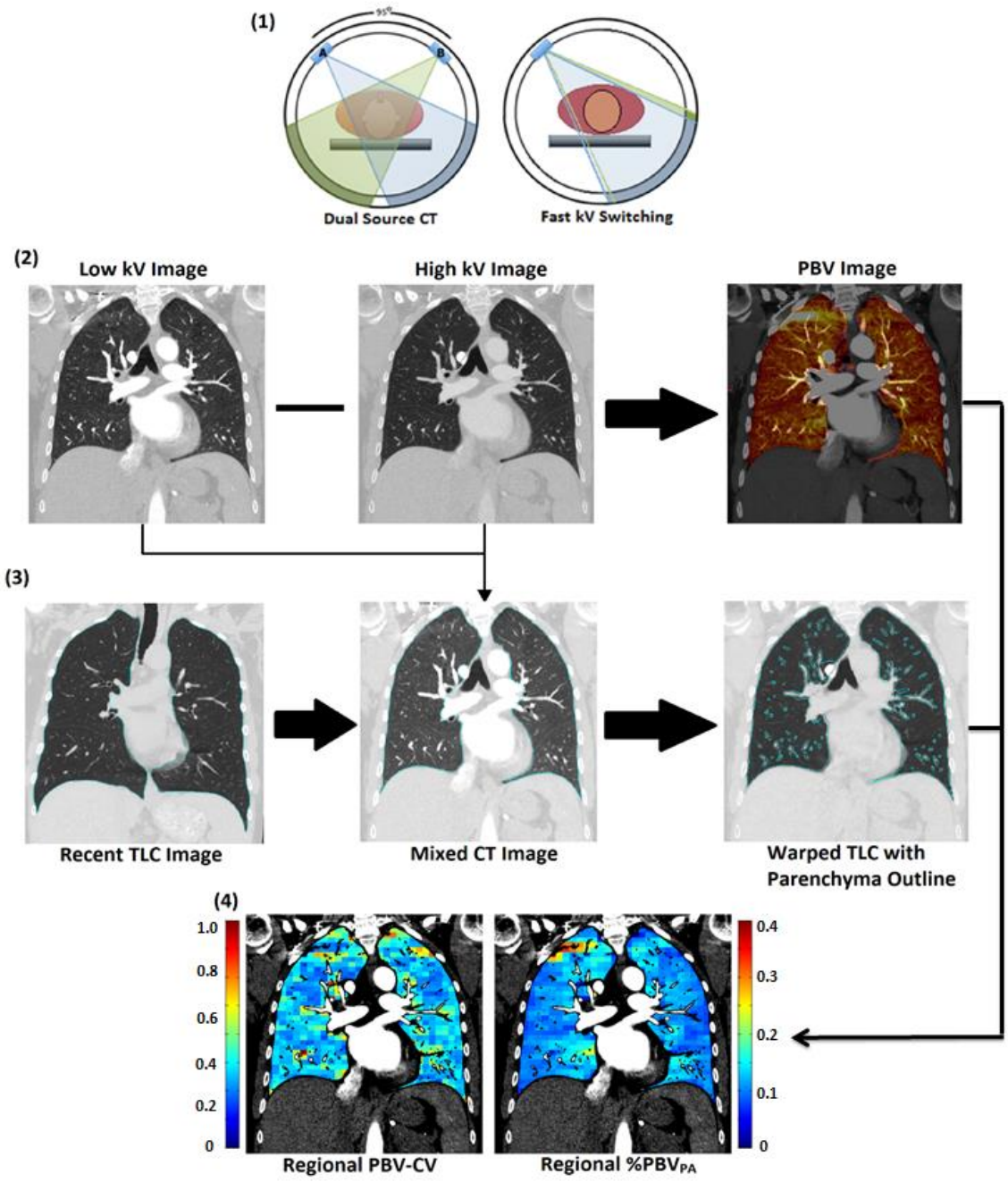

Figure 16: Dual energy PBV imaging acquisition, processing and regional analysis. (1) PBV imaging is performed with one of two methods: dual source (left) or fast kV switching (right), acquiring low and high energy contrast-enhanced images. (2) Scanner associated three-material decomposition is performed on the high and low energy images to generate the PBV map. (3) The most recent TLC image is registered to the mixed CT image (generated from high and low energy images) and warped TLC lung segmentation excluding vessels and airways is acquired. (4) PBV overlay is regionalized and PBV-CV and %PBV$_{PA}$ region maps are created.

Table 9: Subject characteristics and CT-derived data in GE, Flash and Force groups are reported as mean ± standard deviation with the exception of N and sex. N, number of subjects; BMI, body mass index; FEV_1, forced expiratory volume in 1 second; FVC, forced vital capacity; FRC, functional residual capacity; EI, emphysema index (evaluated on TLC image). GE vs. Force, * $p < 0.05$; Flash vs. GE, $^{\#}$ $p < 0.05$; Force vs. Flash, $^{\$}$ $p < 0.05$

Subject characteristics as predictors of PBV-CV in a multi linear regression model			
Characteristic	GE	Siemens Flash	Siemens Force
N	45	17	18
Sex (% male)	60	24	33
Age (years) *$^{\#\$}$	65.8 ± 6.7	46.2 ± 9.2	55.4 ± 9.0
BMI (kg/m^2) $^{\$}$	29.0 ± 4.9	26.1 ± 4.1	30.0 ± 4.9
Pack years $^{\#\$}$	51.3 ± 22.7	22.7 ± 14.8	46.7± 29.0
% Predicted FEV_1 $^{\#\$}$	97.2 ± 11.0	118.1 ± 19.2	96.0 ± 18.3
FEV_1/FVC (%) *$^{\#}$	68.6 ± 8.7	81.0 ± 12.4	75.0 ± 5.8
FRC Volume (L)	3.32 ± 0.83	3.60 ± 0.78	3.01 ± 0.74
EI (TLC) *$^{\#}$	4.52 ± 4.6	0.36 ± 0.3	2.07 ± 2.5

Table 10: Regional $\%PBV_{PA}$ and PBV-CV measurements in GE, Force and Flash subjects. Results are reported as mean ± standard deviation.

		30x30x40 regions		Fixed region size	
Metric	Group	Non-Warp	Warp	Non-Warp	Warp
$\%PBV_{PA}$	GE	0.208 ± 0.05*	0.186 ± 0.04	0.212 ± 0.05*	0.188 ± 0.04
	Force	0.165 ± 0.05	0.166 ± 0.05	0.169 ± 0.05	0.169 ± 0.05
	Flash	0.190 ± 0.03	0.190 ± 0.03	0.191 ± 0.03	0.191 ± 0.03
PBV-CV	GE[#$]	0.607 ± 0.05	0.546 ± 0.05	0.605 ± 0.05	0.546 ± 0.05
	Force[$&]	0.450 ± 0.07	0.449 ± 0.07	0.460 ± 0.07	0.460 ± 0.07
	Flash[&#]	0.360 ± 0.05	0.360 ± 0.06	0.372 ± 0.05	0.372 ± 0.05

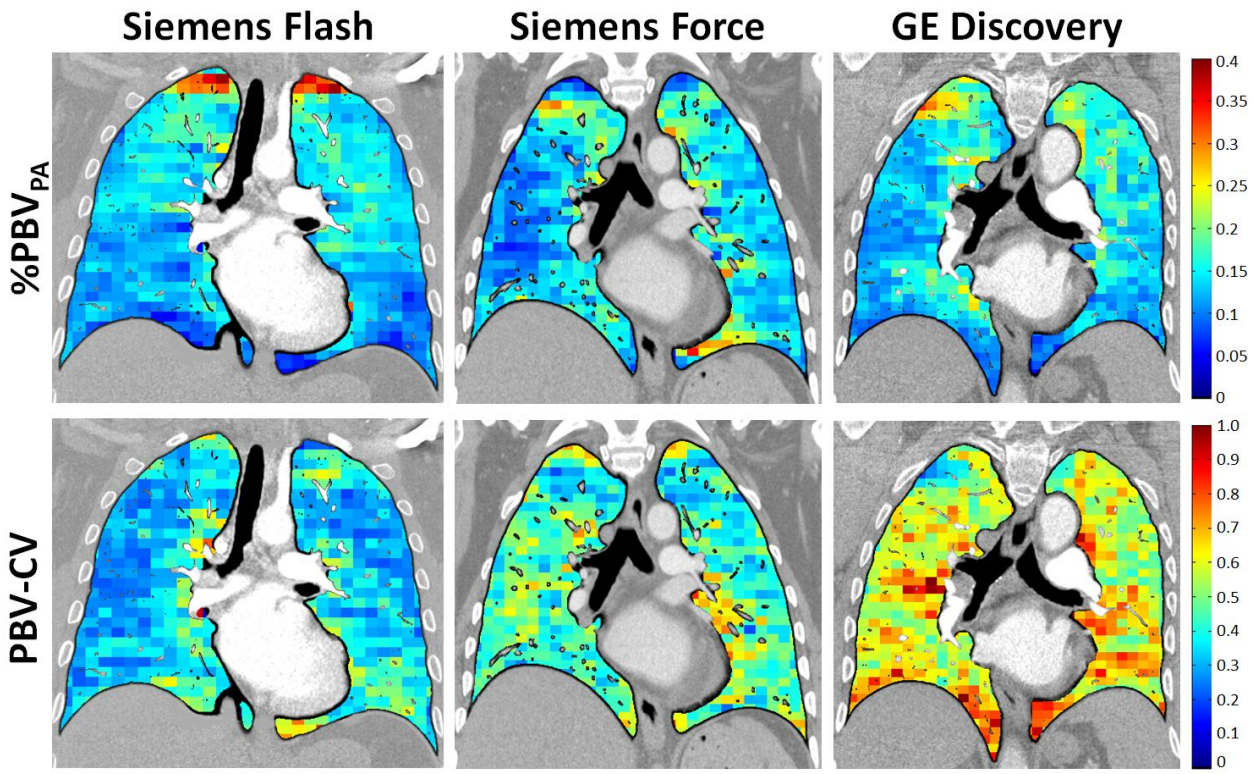

Figure 17: Regional %PBVPA (top) and PBV-CV (bottom) overlaid on mixed CT image in (left) Siemens SOMATOM Definition Flash, (middle) Siemens SOMATOM Force and (right) GE Discovery 750 HD.

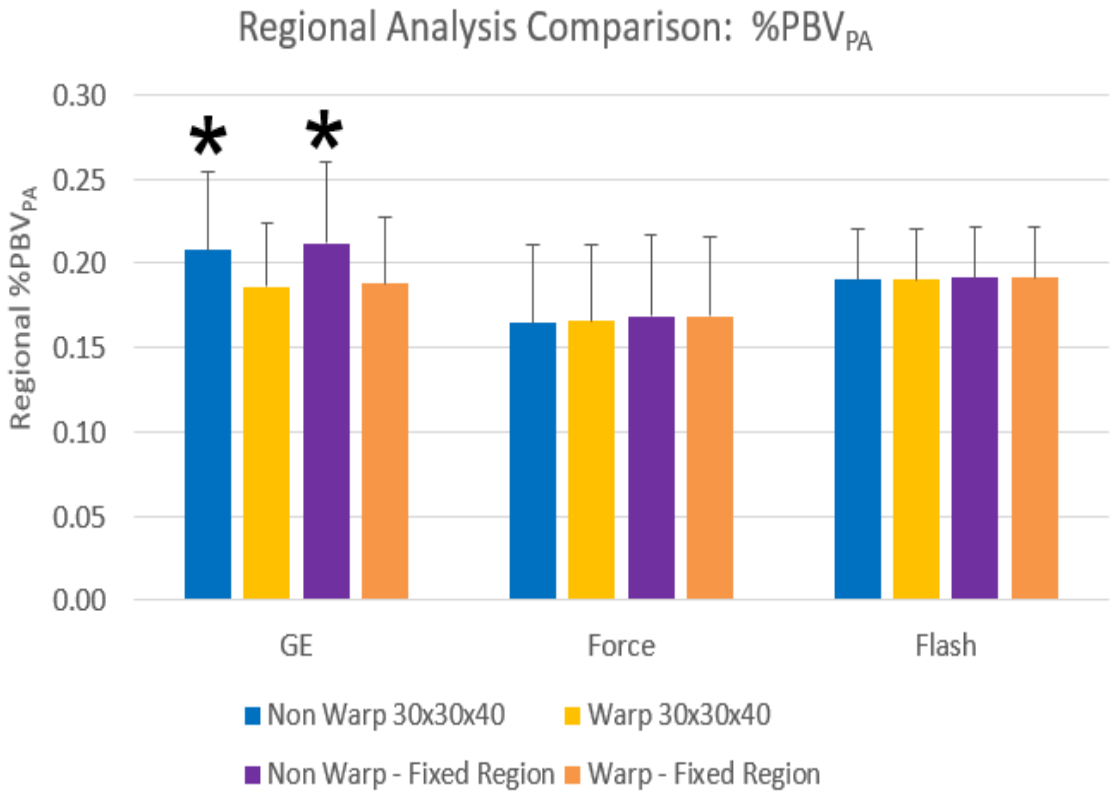

Figure 18: Comparison of regional %PBV$_{PA}$ among regional analysis methods used in this analysis. Non-warped GE differed from non-warped Force regional %PBV$_{PA}$ ($p < 0.01$) and from warped GE %PBV$_{PA}$ ($p < 0.001$)

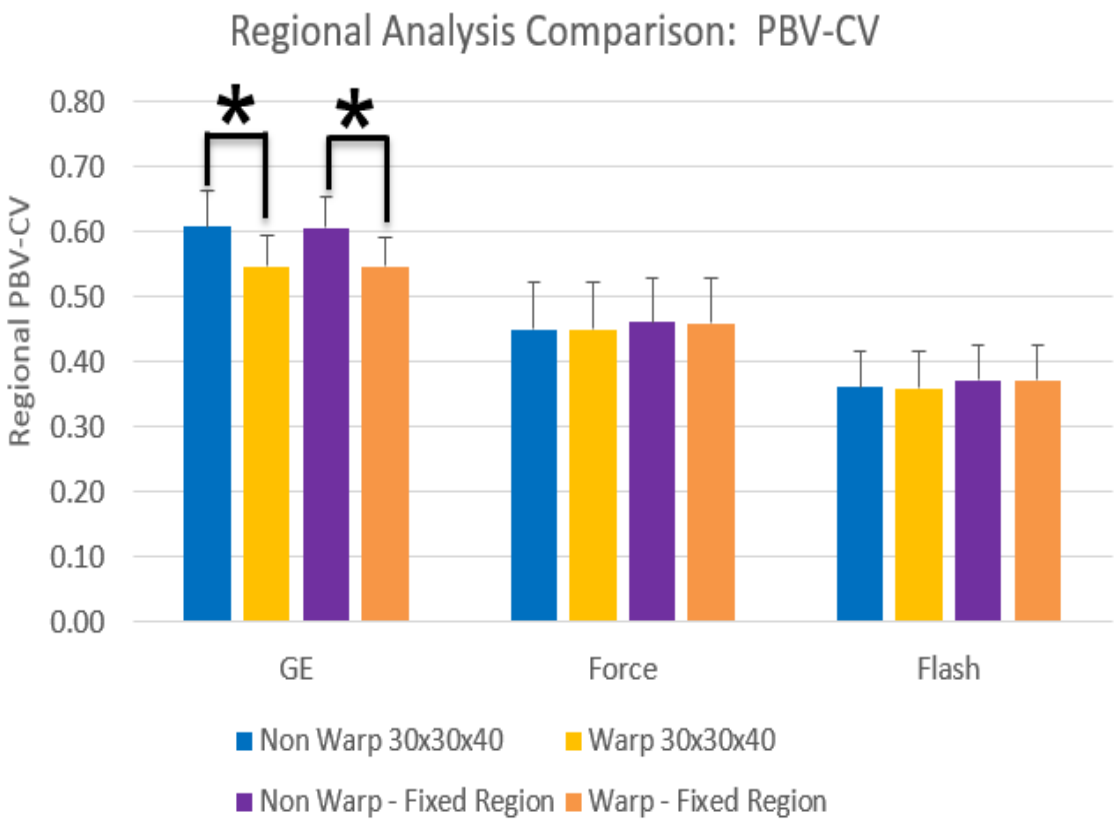

Figure 19: Comparison of regional PBV-CV among regional analysis methods used in this analysis. All three groups differed from one another, but only in the GE group did non-warped and warped PBV images differ from one another (* $p < 0.001$).

Table 11: Summary of multi-linear regression model with stepwise selection in non-warped 30x30x40 region model. The system used to acquire the images was the most important factor in predicting PBV-CV, while contrast concentration, BMI and FRC volume were also important factors.

Non-warped 30 x 30 x 40 region multi-linear regression model				
Feature	**Estimate**	**Std. Error**	**t-value**	**p-value**
Intercept	0.643	0.048	13.4	<< 0.001
Flash	-0.233	0.012	-19.8	<< 0.001
Force	-0.243	0.020	-12.1	<< 0.001
Male	0.053	0.009	5.92	<< 0.001
PBV (100 μg/ml)	-0.005	0.001	-5.75	<< 0.001
BMI (kg/m^2)	0.004	0.001	4.29	<< 0.001
$R_{adj}^2 = 0.915$, $p < 2.2e\text{-}16$				

Table 12: Summary of multi-linear regression model with stepwise selection in warped 30x30x40 region model. The system used to acquire the images was the most important factor in predicting PBV-CV, while contrast concentration, BMI and FRC volume were also important factors.

Warped 30 x 30 x 40 region multi-linear regression model				
Feature	**Estimate**	**Std. Error**	**t-value**	**p-value**
Intercept	0.645	0.051	12.72	<< 0.001
Flash	-0.146	0.011	-13.25	<< 0.001
Force	-0.183	0.018	-10.38	<< 0.001
PBV (100 μg/ml)	-0.069	0.001	-6.50	<< 0.001
Male	0.046	0.008	5.58	<< 0.001
BMI (kg/m^2)	0.004	0.001	4.78	<< 0.001
% Predicted FEV_1	-0.047	0.024	-1.92	0.0593
$R_{adj}^2 = 0.887$, $p < 2.2e\text{-}16$				

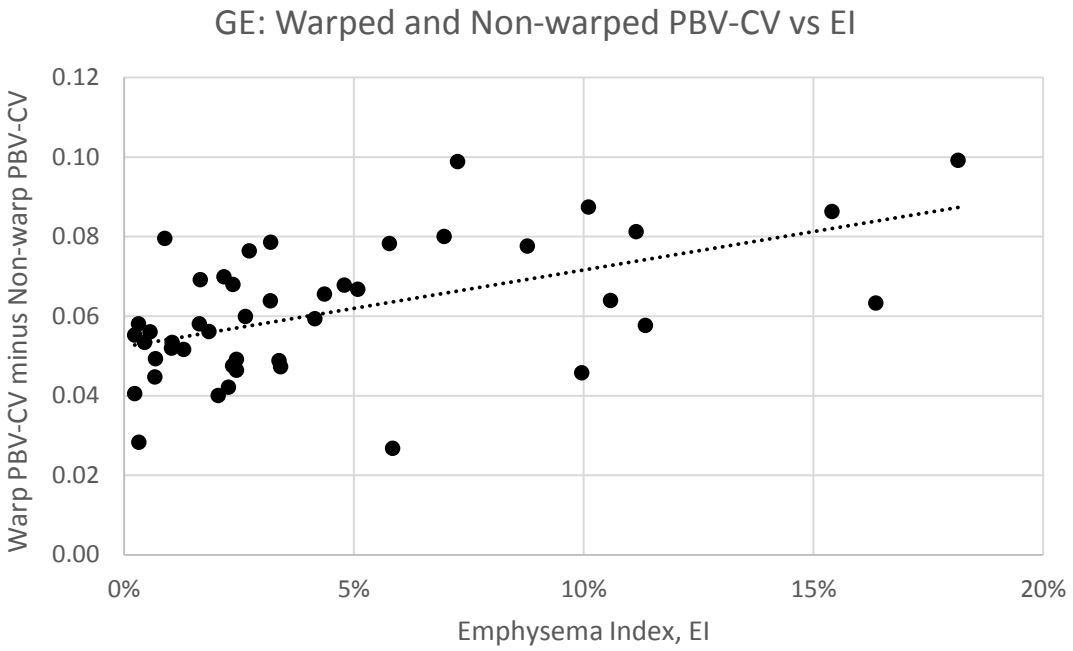

Figure 20: Difference between warped and non-warped PBV-CV vs emphysema index in GE subjects. A statistically significant positive correlation was observed ($R = 0.5315$, $p < 0.001$).

CHAPTER 5: CONCLUSIONS & FUTURE WORK

In Chapter 2, we identified rapid and non-rapid emphysema progressors from within the SPIROMICS cohort and used a custom built GUI to measure central pulmonary arterial cross sectional area normalized to the associated airway segment area. We concentrated on the level of the segmental airways and used airway-artery pairs previously demonstrated to have the greatest measurement reliability. We demonstrated that rapid progressors had enlarged normalized pulmonary arterial areas and that the normalized measurement, CSA_{Norm} was related to FEV_1/FVC, % predicted FEV_1 and EI, which are all metrics of COPD severity. This is as one would expect if the arterial metric is associated with a more rapid progression of the disease. Because of the fact that the increased normalized arterial metrics have been found within normal smokers [4] shown to have emphysema susceptibility, we believe that the arterial signal is a sign of vascular dysfunction and not a result of peripheral destruction. Iyer et al. [4] has shown that the normalized arterial cross sectional differences between emphysema susceptible and non-susceptible subjects are reversible with sildenafil. Our findings coupled with the earlier findings [3, 4] suggest that the peripheral vasoconstriction is a causal factor in the rapid progression of emphysema in some smokers. More specifically, we think these findings relate to increased downstream vascular resistance related to an inability to block the HPV response in the presence of lung inflammation. In future studies, we would like to perform this analysis in FRC scans of smoking subjects with COPD. The imaging protocol for SPIROMICS only included TLC and RV scans. Our concern with the TLC images was that the blood vessels would be stretched from the large lung volumes. We did attempt to make these measurements in RV scans, but these proved to be too

unreliable for a number of reasons including poor lung volume control, excessive image noise/motion and a lack of associated airway measurements. Currently, this analysis is being expanded to the remaining SPIROMICS subjects in order to study trends across the entire study cohort.

In Chapter 3, we attempted to develop a DECT PBV imaging protocol in a large animal model with contrast dilution and reduced radiation does to be implemented in future human imaging studies. We analyzed several radiation doses across six pigs with a contrast/saline ratio of 50/50 and used PBV metrics: $\%PBV_{PA}$ and PBV-CV in order to analyze the effects of radiation dose reduction on PBV imaging. We found that radiation dose does have a significant effect on PBV-CV, but it is of secondary importance to the iodine signal in the pulmonary circulation. The iodine signal is related to the timing of the contrast injection and CT scanning commencement as well as cardiac output and the concentration of iodine injection. We reduced radiation dose from 11.3 mGy to 7.47 mGy, which translates to approximately 5.3 mSv and 3.5 mSv in this study, without compromising our PBV-CV measurement. We are currently collecting data (some of which was presented in Chapter 4) in a multi-center study where two sites have reduced the contrast to 50/50 contrast/saline. In future human studies, we would like to implement a low radiation dose DECT PBV scan with diluted contrast.

In Chapter 4, we studied the effect of scanner model on PBV-CV. We analyzed PBV images from three DECT scanners: two Siemens systems (Flash and Force) with dual source and on GE system (Discovery 750 HD) with fast kV switching. We demonstrated that PBV-CV measured in subjects scanned with the GE system was increased and that we could not account for the difference solely with subject specific

characteristics. This led us to conclude that increased image noise from the fast kV switching technique is the likely cause of the increase in PBV-CV. In future studies, we would like to use newer iterative reconstruction algorithms in order to remove some of this excessive noise.

REFERENCES

1. Siafakas, N.M., et al., Optimal assessment and management of chronic obstructive pulmonary disease (COPD). The European Respiratory Society Task Force. Eur Respir J, 1995. 8(8): p. 1398-420.

2. Society, A.T., Standards for the diagnosis and care of patients with chronic obstructive pulmonary disease. . Am J Respir Crit Care Med, 1995. 152(5 Pt 2): p. S77-121.

3. Alford, S.K., et al., Heterogeneity of pulmonary perfusion as a mechanistic image-based phenotype in emphysema susceptible smokers. Proc Natl Acad Sci U S A, 2010. 107(16): p. 7485-90.

4. Iyer, K.S., et al., Quantitative Dual-Energy Computed Tomography Supports a Vascular Etiology of Smoking-induced Inflammatory Lung Disease. Am J Respir Crit Care Med, 2016. 193(6): p. 652-61.

5. Couper, D., et al., Design of the Subpopulations and Intermediate Outcomes in COPD Study (SPIROMICS). Thorax, 2014. 69(5): p. 491-4.

6. West, J.B., Respiratory physiology: The essentials. 4th ed1990: Williams & Wilkins.

7. Singhal, S., et al., Morphometry of the human pulmonary arterial tree. Circ Res, 1973. 33(2): p. 190-7.

8. Townsley, M.I., Structure and composition of pulmonary arteries, capillaries, and veins. Compr Physiol, 2012. 2(1): p. 675-709.

9. Pauwels, R.A., et al., Global strategy for the diagnosis, management, and prevention of chronic obstructive pulmonary disease. NHLBI/WHO Global Initiative for Chronic Obstructive Lung Disease (GOLD) Workshop summary. Am J Respir Crit Care Med, 2001. 163(5): p. 1256-76.

10. West, J.B., Pulmonary pathophysiology: The essentials. 5th ed1998: Williams & Wilkins.

11. Barr, R.G., The epidemiology of vascular dysfunction relating to chronic obstructive pulmonary disease and emphysema. Proc Am Thorac Soc, 2011. 8(6): p. 522-7.

12. Barr, R.G., et al., Percent emphysema, airflow obstruction, and impaired left ventricular filling. N Engl J Med, 2010. 362(3): p. 217-27.

13. Grout RW, A.S., Barr RG, Hoffman EA. Total pulmonary vascular volume: A new copd phenotype correlated with quantitative ct and pft measures of emphysema. in American Thoracic Society. 2010. New Orleans.

14. Matsuoka, S., et al., Quantitative CT measurement of cross-sectional area of small pulmonary vessel in COPD: correlations with emphysema and airflow limitation. Acad Radiol, 2010. 17(1): p. 93-9.

15. Peinado, V.I., et al., Pulmonary vascular abnormalities in chronic obstructive pulmonary disease undergoing lung transplant. J Heart Lung Transplant, 2013. 32(12): p. 1262-9.

16. Peinado, V.I., S. Pizarro, and J.A. Barbera, Pulmonary vascular involvement in COPD. Chest, 2008. 134(4): p. 808-14.

17. Wells, J.M., et al., Pulmonary arterial enlargement and acute exacerbations of COPD. N Engl J Med, 2012. 367(10): p. 913-21.

18. Santos, S., et al., Characterization of pulmonary vascular remodelling in smokers and patients with mild COPD. Eur Respir J, 2002. 19(4): p. 632-8.

19. Peinado, V.I., et al., Inflammatory reaction in pulmonary muscular arteries of patients with mild chronic obstructive pulmonary disease. Am J Respir Crit Care Med, 1999. 159(5 Pt 1): p. 1605-11.

20. Peinado, V.I., et al., Endothelial dysfunction in pulmonary arteries of patients with mild COPD. Am J Physiol, 1998. 274(6 Pt 1): p. L908-13.

21. Kalender, W.A., et al., Spiral volumetric CT with single-breath-hold technique, continuous transport, and continuous scanner rotation. Radiology, 1990. 176(1): p. 181-3.

22. Hoffman, E.A., B.A. Simon, and G. McLennan, State of the Art. A structural and functional assessment of the lung via multidetector-row computed tomography: phenotyping chronic obstructive pulmonary disease. Proc Am Thorac Soc, 2006. 3(6): p. 519-32.

23. Busacker, A., et al., A multivariate analysis of risk factors for the air-trapping asthmatic phenotype as measured by quantitative CT analysis. Chest, 2009. 135(1): p. 48-56.

24. Dournes, G., et al., Computed tomographic measurement of airway remodeling and emphysema in advanced chronic obstructive pulmonary disease. Correlation with pulmonary hypertension. Am J Respir Crit Care Med, 2015. 191(1): p. 63-70.

25. Kim, Y.I., et al., Gender differences of airway dimensions in anatomically matched sites on CT in smokers. Copd, 2011. 8(4): p. 285-92.

26. Chiro, G.D., et al., Tissue signatures with dual-energy computed tomography. Radiology, 1979. 131(2): p. 521-3.

27. Genant, H.K. and D. Boyd, Quantitative bone mineral analysis using dual energy computed tomography. Invest Radiol, 1977. 12(6): p. 545-51.

28. Fornaro, J., et al., Dual- and multi-energy CT: approach to functional imaging. Insights Imaging, 2011. 2(2): p. 149-159.

29. Wagner, P.D., et al., Continuous distributions of ventilation-perfusion ratios in normal subjects breathing air and 100 per cent O2. J Clin Invest, 1974. 54(1): p. 54-68.

30. Wagner, P.D., H.A. Saltzman, and J.B. West, Measurement of continuous distributions of ventilation-perfusion ratios: theory. J Appl Physiol, 1974. 36(5): p. 588-99.

31. Glenny, R.W., et al., Temporal heterogeneity of regional pulmonary perfusion is spatially clustered. J Appl Physiol (1985), 1995. 79(3): p. 986-1001.

32. Glenny, R.W. and H.T. Robertson, Fractal properties of pulmonary blood flow: characterization of spatial heterogeneity. J Appl Physiol (1985), 1990. 69(2): p. 532-45.

33. Gust, R., et al., Synergistic hemodynamic effects of low-dose endotoxin and acute lung injury. Am J Respir Crit Care Med, 1998. 157(6 Pt 1): p. 1919-26.

34. Schuster, D.P. and G.F. Marklin, Effect of changes in inflation and blood volume on regional lung density--a PET study: 2. J Comput Assist Tomogr, 1986. 10(5): p. 730-5.

35. Velazquez, M. and D.P. Schuster, Perfusion redistribution after alveolar flooding: vasoconstriction vs. vascular compression. J Appl Physiol (1985), 1991. 70(2): p. 600-7.

36. Chon, D., et al., Regional pulmonary blood flow in dogs by 4D-X-ray CT. J Appl Physiol (1985), 2006. 101(5): p. 1451-65.

37. Hoffman, E.A., J.K. Tajik, and S.D. Kugelmass, Matching pulmonary structure and perfusion via combined dynamic multislice CT and thin-slice high-resolution CT. Comput Med Imaging Graph, 1995. 19(1): p. 101-12.

38. Won, C., et al., CT-based assessment of regional pulmonary microvascular blood flow parameters. J Appl Physiol (1985), 2003. 94(6): p. 2483-93.

39. Fuld, M.K., et al., Pulmonary perfused blood volume with dual-energy CT as surrogate for pulmonary perfusion assessed with dynamic multidetector CT. Radiology, 2013. 267(3): p. 747-56.

40. Schlomka, J.P., et al., Experimental feasibility of multi-energy photon-counting K-edge imaging in pre-clinical computed tomography. Phys Med Biol, 2008. 53(15): p. 4031-47.

41. Liu, X., et al., Quantitative imaging of element composition and mass fraction using dual-energy CT: three-material decomposition. Med Phys, 2009. 36(5): p. 1602-9.

42. Barr, R.G., et al., Impaired flow-mediated dilation is associated with low pulmonary function and emphysema in ex-smokers: the Emphysema and Cancer Action Project (EMCAP) Study. Am J Respir Crit Care Med, 2007. 176(12): p. 1200-7.

43. Ferrer, E., et al., Effects of cigarette smoke and hypoxia on pulmonary circulation in the guinea pig. Eur Respir J, 2011. 38(3): p. 617-27.

44. Jin, D., et al. A semi-automatic framework of measuring pulmonary arterial metrics at anatomic airway locations using CT imaging. 2016.

45. Regan, E.A., et al., Genetic epidemiology of COPD (COPDGene) study design. Copd, 2010. 7(1): p. 32-43.

46. Shikata, H., et al., Segmentation of Pulmonary Vascular Trees from Thoracic 3D CT Images. Int J Biomed Imaging, 2009. 2009: p. 636240.

47. Hoffman, E.A., et al., Reproducibility and validity of lung density measures from cardiac CT Scans--The Multi-Ethnic Study of Atherosclerosis (MESA) Lung Study. Acad Radiol, 2009. 16(6): p. 689-99.

48. Choi, S., et al., Registration-based assessment of regional lung function via volumetric CT images of normal subjects vs. severe asthmatics. J Appl Physiol (1985), 2013. 115(5): p. 730-42.

49. Iyer, K.S., et al., Repeatability and Sample Size Assessment Associated with Computed Tomography-Based Lung Density Metrics. Chronic Obstr Pulm Dis (Miami), 2014. 1(1): p. 97-104.

50. Fuld, M.K., et al., CT-measured regional specific volume change reflects regional ventilation in supine sheep. J Appl Physiol (1985), 2008. 104(4): p. 1177-84.

51. Kong, X., et al., Xenon-enhanced dual-energy CT lung ventilation imaging: techniques and clinical applications. AJR Am J Roentgenol, 2014. 202(2): p. 309-17.

52. Nakazawa, T., et al., Lung perfused blood volume images with dual-energy computed tomography for chronic thromboembolic pulmonary hypertension: correlation to scintigraphy with single-photon emission computed tomography. J Comput Assist Tomogr, 2011. 35(5): p. 590-5.

53. Zhang, L.J., et al., Dual-energy CT lung ventilation/perfusion imaging for diagnosing pulmonary embolism. Eur Radiol, 2013. 23(10): p. 2666-75.

54. Yin, Y., et al., A cubic B-spline-based hybrid registration of lung CT images for a dynamic airway geometric model with large deformation. Phys Med Biol, 2011. 56(1): p. 203-18.

55. Yin, Y., E.A. Hoffman, and C.L. Lin, Mass preserving nonrigid registration of CT lung images using cubic B-spline. Med Phys, 2009. 36(9): p. 4213-22.